CATÓLICA
FACULTY OF BIOTECHNOLOGY

PORTO

INTEGRATION OF SOFT TISSUES WITH INTRAOSSEOUS PROSTHESES: A TISSUE ENGINEERING APPROACH

by

José Miguel Sousa Lima

November 2024

CATÓLICA
FACULTY OF BIOTECHNOLOGY
PORTO

INTEGRATION OF SOFT TISSUES WITH INTRAOSSEOUS PROSTHESES: A TISSUE ENGINEERING APPROACH

Thesis presented to *Escola Superior de Biotecnologia* of the *Universidade Católica Portuguesa* to fulfill the requirements of Master of Science degree in Biomedical Engineering

by

José Miguel Sousa Lima

Supervisor: Doctor Francesca Scalera

Co-supervisor: Doctor Clara Piccirillo

Tutor (University): Doctor Viviana Ribeiro

November 2024

Resumo

Melhorar a qualidade de vida de indivíduos com amputação de membros inferiores é um objetivo fundamental no desenvolvimento e na reabilitação de próteses. Biomateriais que replicam as propriedades do tecido natural podem desempenhar um papel essencial na melhoria da integração e funcionalidade das próteses. Este trabalho centra-se na síntese e caracterização de criogéis à base de Gelatina Metacrilada (GelMA), especificamente desenhados para potenciar a integração do tecido mole com próteses transcutâneas osseointegradas para membros inferiores.

Foram empregues reações de metacrilação para criar derivados de GelMA e CsMA, com níveis de metacrilação de 55% e 16%, respetivamente, confirmados através de espectroscopia de infravermelho com transformada de Fourier (FTIR) e ensaios de ninidrina. A otimização das formulações incluiu a incorporação de Diacrilato de Polietilenoglicol (PEGDA) e Pectina com GelMA. Avaliações de estabilidade destacaram o efeito estabilizador superior do PEGDA, com os criogéis de GelMA_PEGDA a apresentarem apenas 20% de perda de peso ao longo de 14 dias, em comparação com os 40% do GelMA. Em contraste, as formulações de GelMA_Pectina degradaram-se rapidamente. Testes de *swelling* indicaram que o aumento da reticulação conferido pelo PEGDA reduziu a absorção de água, resultando num comportamento de inchaço controlado, adequado para aplicações sensíveis à humidade. A análise por Microscopia Eletrónica de Varrimento (SEM) mostrou uma rede porosa em todos os criogéis, com GelMA_PEGDA a apresentar poros menores e mais uniformes — uma estrutura ideal para promover a infiltração celular. Os testes mecânicos reforçaram o potencial dos criogéis de GelMA_PEGDA, revelando propriedades viscoelásticas melhoradas e uma elevada resistência à compressão, ambas cruciais para aplicações de tecido que suportam carga. Após refinamentos nos protocolos de preparação, os criogéis de GelMA_PEGDA apresentaram uma elevada biocompatibilidade, comprovada pela substancial viabilidade e proliferação celular.

No geral, os criogéis de GelMA_PEGDA apresentam uma combinação promissora de estabilidade, resistência mecânica e biocompatibilidade, tornando-os adequados para investigações adicionais como *scaffolds* para suportar a integração de tecido mole com o implante em próteses transcutâneas de membros inferiores.

Palavras-chave: Amputação de membros inferiores, integração, Gelatina Metacrilada, Diacrilato de Polietilenoglicol, criogéis

Abstract

Enhancing the quality of life for individuals with lower limb amputation is a fundamental goal in prosthetic development and rehabilitation. Biomaterials that replicate the properties of natural tissue can play a pivotal role in improving the integration and functionality of prostheses. This thesis focuses on the synthesis and characterization of cryogels based on Gelatin Methacrylate (GelMA), designed specifically to enhance the integration of soft tissue with osseointegrated transcutaneous lower limb prostheses.

Methacrylation reactions were employed to create GelMA and CsMA derivatives, with methacrylation levels reaching 55% and 16%, respectively, as confirmed through Fourier-transform infrared (FTIR) spectroscopy and ninhydrin assays. Further optimization included incorporating Polyethylene Glycol Diacrylate (PEGDA) and Pectin with GelMA. Stability assessments highlighted the superior stabilizing effect of PEGDA, with GelMA_PEGDA cryogels exhibiting only 20% weight loss over 14 days compared to 40% for GelMA alone. By contrast, GelMA_Pectin formulations degraded quickly. Swelling tests indicated that the increased crosslinking conferred by PEGDA reduced water uptake, resulting in controlled swelling behavior suitable for moisture-sensitive applications. Scanning Electron Microscopy (SEM) analysis showed a porous network in all cryogels, with GelMA_PEGDA presenting smaller, more uniform pores—an ideal structure for promoting cell infiltration. Mechanical testing further supported the potential of GelMA_PEGDA cryogels, revealing enhanced viscoelastic properties and strong compressive strength, both of which are crucial for load-bearing tissue applications. Following refinements in preparation protocols, the GelMA_PEGDA cryogels exhibited high biocompatibility, as evidenced by substantial cell viability and proliferation rates.

Overall, GelMA_PEGDA cryogels exhibit a promising combination of stability, mechanical strength, and biocompatibility, making them well-suited for further investigation as scaffolds to support soft tissue integration with the abutment in transcutaneous lower limb prostheses.

Keywords: Lower limb amputation, integration, Gelatin Methacrylate, Polyethylene Glycol Diacrylate, cryogels

Acknowledgements

First and foremost, I would like to express my gratitude to my supervisor, Dr. Francesca Scalera, for giving me the opportunity to work on this project and for the guidance she has offered me during the five months I was fortunate to spend at the CNR Nanotec in Lecce, Italy. This has enabled me to learn and progress in the lab with great ease.

I am equally thankful to my co-supervisor, Dr. Clara Piccirillo, for welcoming me and offering her help during the entire period I spent in Italy. Her assistance made the task at hand both enjoyable and productive.

I would like to express my deepest gratitude to my lovely girlfriend, whose company and unwavering support made this experience abroad even more fulfilling. Her encouragement, patience and assurance have been invaluable, especially during the most challenging moments of this journey. Her presence has been a source of strength, motivation, and joy.

I am also appreciative of all my friends who have been by my side throughout this journey, consistently showing interest in my work and cheering me on every step of the way.

On this note, the *Tuna da Universidade Católica Portuguesa - Porto* is something I would like to acknowledge for providing me with an outlet to relax during my time working on this thesis. The music and camaraderie offered an escape from the stresses of my research.

Last but by no means least, I extend my heartfelt thanks to my parents, my brother and my family as a whole for their unconditional support and encoragement, for providing me the means to pursue this degree and for always showing enthusiasm and genuine care about my research. Their belief in me has been a source of strength and motivation.

Table of Contents

Figure List

Table List

List of abbreviations

APS - Ammonium Persulfate

bFGF - Basic Fibroblast Growth Factor

Cs - Chitosan

CsMA - Chitosan Methacrylate

DMSO - Dimethyl Sulfoxide

DMEM - Dulbecco's Modified Eagle Medium

FBS - Fetal Bovine Serum

FTIR - Fourier Transform Infrared

GelMA - Gelatin Methacrylate

G' - Storage Modulus

G'' - Loss Modulus

ILP - Integral-Leg Prosthesis

ITAP - Intraosseous Transcutaneous Amputation Prostheses

LAP - Lithium Phenyl-2,4,6-Trimethylbenzoylphosphinate

L-Arg - L-Arginine

NO - Nitric Oxide

OD - Optical Density

OPL - Osseointegrated Prosthetic Limb

OPRA - Osseointegrated Prosthesis for the Rehabilitation of Amputees

PBS - Phosphate-Buffered Saline

PDGF - Platelet-Derived Growth Factor

PEGDA - Polyethylene Glycol Diacrylate

PI - Propidium Iodide

SEM - Scanning Electron Microscopy

TEMED - N,N,N',N'-Tetramethylethylenediamine

UV - Ultraviolet

VEGF - Vascular Endothelial Growth Factor

1. Introduction

1.1. Challenges and Innovations in Lower Limb Prosthetic Design and Usage

A person's ability to move around and their wellbeing in general is affected significantly when one or both lower limbs is lost. Amputation of the lower extremities whether due to injury, illness, or even birth defects also mandates revising conventional attitudes to the prosthetic limbs in order to improve the health of the patients. In rehabilitation after the loss of a lower limb, assistive technology occupies an essential position, focusing on the restoration of the patient's daily activities and an increase in their life quality. On the contrary, using prostheses may also result in falls and other injuries like low back pain, osteoarthritis of the normal knee, and hip joints, which causes higher expenses for medical care and diminishes the overall satisfaction of life. Hence, it is important to note that designs of titanium prosthetic limbs for amputees significantly aid mobility, performance of daily living activities, and most importantly, the psychological and social wellbeing of the individuals.

Performance and comfort in prosthetic devices depend greatly on the correct load distribution and load-bearing capacities. In this sense, one of the most complicated challenges facing the field of prosthetics is the human-prosthetic interface.

Dr. Sidney Fishman, in the first volume of the Journal of Prosthetics and Orthotics, which is the official publication of the International Society for Prosthetics and Orthotics published in 1977, insisted on the need for providing institutional training and education to reinforce the practical work of prosthetists and orthotists to a satisfactory level, especially in the biological sciences. He further stated that the design of prosthetic devices would not only be dependent on creativity but would also involve a thorough comprehension of biomechanics as well as soft tissue mechanics [1].

Despite the progress of the last four decades, the interface between the human body and prosthetic devices remains a major challenge.

In order for a prosthesis to be efficient it should achieve a good fit with the bones within the user's body for efficient movement control without inflicting pain or discomfort in any way. This is usually done in the form of a socket which helps in attaching the prosthesis into the skeletal structure of the individual through the soft tissues of the residual limb. However, it is estimated that up to 50% of individuals with transtibial amputations do not regularly use their prostheses, largely due to socket-related issues [25]. This rate of disuse is even higher among individuals with transfemoral amputations [26]. The primary complaints regarding prostheses

involve discomfort from the socket and poor socket fit, which can lead to skin problems [27]. These issues are usually exacerbated with variations in the residual limb volume over time [28], in addition to heat and perspiration within the confined socked space [29]. Currently, prosthetic manufacturing is largely empirical rather than data-driven; it is an iterative, labour-intensive process that depends heavily on the skill and experience of the prosthetist, as well as input from the amputee. One of the major developments in the last few decades has been the osseointegration (OI), which allows improved functionality, mobility and enhanced quality of life for some amputation patients who are intolerant of traditional sockets. Despite its benefits, OI usage is limited due to risks such as infection, implant failure, and osteomyelitis [30].

1.2. Overview of Osteointegrated Lower Limb Prostheses

Osseointegration is the direct structural and functional bonding between living bone and the surface of an artificial metal implant [31], allowing for stable fixation between remodelled biological tissues and a titanium implant without triggering rejection mechanisms [32]. In the 1950s, Per-Ingvar Brånemark used a titanium implant chamber to study blood flow in rabbit bone and observed that the chambers could not be removed at the conclusion of the experiment [33]. This significant discovery that bone can integrate with titanium components led him to coin the term osseointegration.

Direct skeletal fixation through osseointegration is currently employed in total joint replacements, dental implants, edentulous mandibles, craniofacial reconstructions, maxillofacial reconstruction, orbital prostheses, and bone-anchored hearing aids. Since the 1990s, it has also been used for percutaneous implants to attach prosthetic limbs. The application of osseointegrated prosthetic implants for limb amputation is now practiced in several centres worldwide, with various approaches to osseointegration having developed and evolved over recent years [34].

There are various types of osteointegrated lower limb prostheses, each with unique features and benefits designed to enhance mobility and improve the quality of life for amputees. Among these, osseointegrated prostheses represent a significant advancement. This section explores three notable systems: the OPRA, the Compress implant, and the OPL along with the ILP. These systems offer different approaches to integrating prosthetic limbs with the residual bone, aiming to provide better stability, comfort, and functionality for users.

1.2.1. The Osseointegrated Prosthesis for the Rehabilitation of Amputees (OPRA)

The OPRA system consists of three components: the fixture, a threaded, cylindrical implant that integrates with the residual bone; the abutment, a percutaneous component that press-fits into the distal end of the fixture to allow attachment to the external prosthesis; and the abutment screw, which connects the fixture to the abutment (Figure 1) [2]. The OPRA fixture includes radially placed perforations along its threaded body, enhancing torsional stability and allowing implantation in short residuum [3].

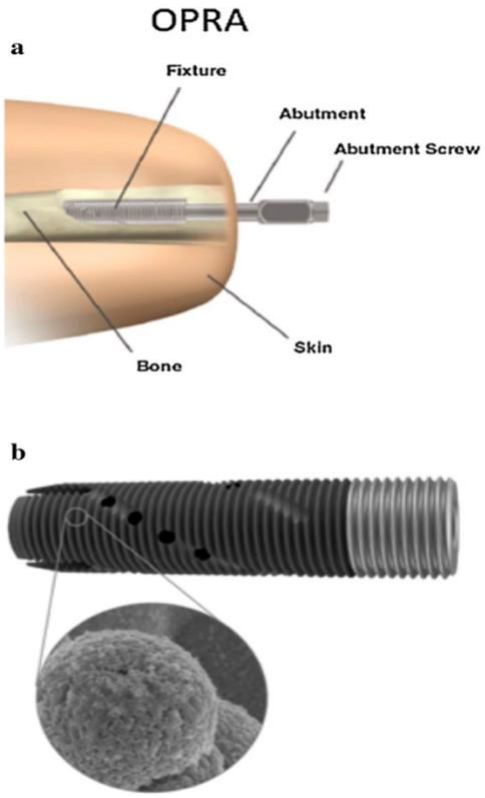

Figure 1 - a) Schematic of the OPRA implant system components; b) The OPRA fixture; the exterior surface undergoes a treatment to improve osseointegration. The lower image provides a detailed view of the microstructure after laser treatment [4].

The OPRA device is implanted in a two-stage surgical process [5]. Initially, the fixture is placed into the medullary canal of the residual bone, and the distal end is augmented with bone graft from the limb or iliac crest, followed by soft tissue closure. In the second stage, the soft tissue is defatted, thinned, and a stoma is created for the percutaneous abutment to connect to the fixture (Figure 2). The soft tissue is then tightly secured to the distal surface of the residual bone to prevent sheering.

The success of the OPRA device is partly due to its revised rehabilitation protocol. Initially, a rapid loadbearing protocol led to implant loosening and revision surgeries [5]. The

protocol was updated to a gradual loading approach, preventing micromotion and allowing for continued bone remodelling, which increased implant survivorship from 40% to 80% [6, 7].

The OPRA device is one of the most extensively studied clinical systems and the only implant approved by the Food and Drug Administration (FDA) under a Humanitarian Device Exemption for treating transfemoral amputees. It is studied for both upper and lower extremities and has shown favourable short- and mid-term survivorship and improved quality of life. Over the past two decades, the implant has seen design enhancements, including a nanoporous surface coating [8], and a fail-safe system where the abutment or screw fractures under excessive load to prevent fixture or bone fractures.

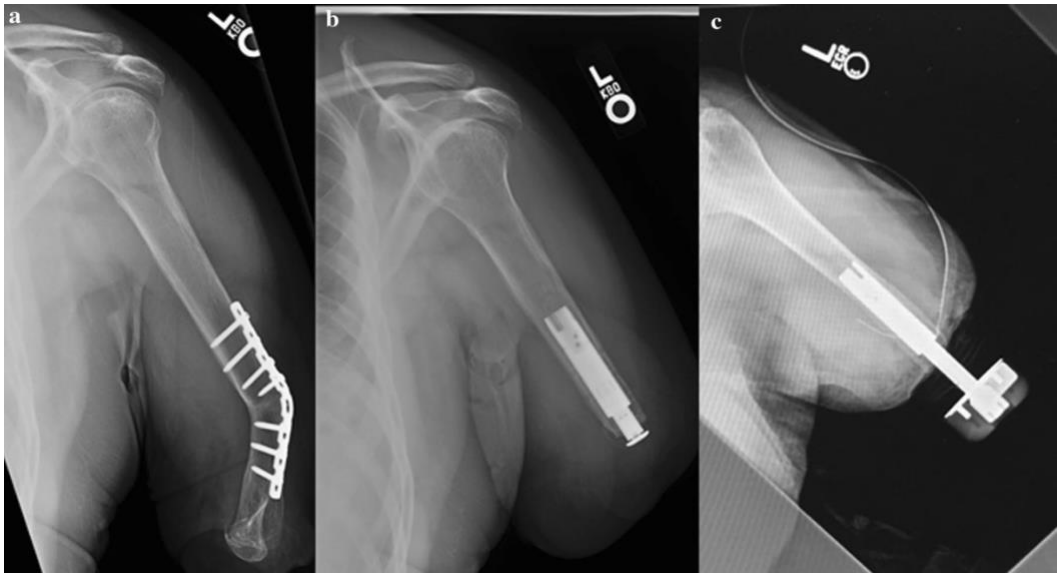

Figure 2 - Preoperative and postoperative radiographs following Stage 1 and Stage 2 of the OPRA Implant System implantation procedure (from left to right) [4].

1.2.2. The Compress

The Compress, originally developed for oncologic limb salvage reconstruction, is an endoprosthetic system that press-fits into the residual bone [8, 9]. Its intramedullary stem is secured with transverse pins, and a spindle applies 600-800 lbs (272-363 kg) of force to the distal end of the residual bone, stimulating growth through Wolff's law and preventing aseptic loosening [10]. Studies show that the Compress has superior survivorship and lower mechanical failure rates compared to other distal femoral replacement implants [11]. It also features a porous titanium collar designed for soft tissue ingrowth and neovascularization.

The Compress implant system effectively mitigates the issue of stress shielding, a common problem with other implants [12, 13]. Stress shielding occurs when an implant absorbs the natural stresses that bones are meant to bear, leading to bone resorption, osteopenia, and

reduced cortical thickness. This phenomenon is closely related to the stiffness of the implant [14, 15] and contributes significantly to the risk of fracture or aseptic loosening [16].

The Compress implant system offers a significant advantage in terms of ease of revision [16]. If an infection occurs, the surgical treatment involves removing less than one centimetre of bone, clearing the infection, and replacing the implant. This procedure is much simpler and less damaging than revising a traditional stem implant, resulting in minimal bone loss. Revising well-fixed orthopaedic implants often requires specialized instruments, such as powered reamers or trephines, which can lead to metal debris, bone loss, and thermal necrosis [18]. Additionally, bone density improves with the compressive load over time [17]. In cases of chronic infection requiring a two-stage revision, the spindle can be retained if it remains well fixed, preserving the primary bone-implant integration, which may not be as robust if the spindle were replaced.

First used for osseointegration in 2012, the Compress implant system has been implanted in eleven amputees - ten transfemoral and one transhumeral – in a study by McGough, R. L. *et al.* (2017). The implants were inserted using either a one- or two-stage surgical approach [14]. Early results were promising, with no infection-related revisions reported. However, two patients experienced periprosthetic fractures due to falls. Further research is necessary to determine the long-term outcomes and survivorship of the Compress implant in osseointegration.

1.2.3. Osseointegrated Prosthetic Limb (OPL) and the Integral-Leg Prosthesis (ILP)

Two similar press-fit fixation implants are in clinical use in Europe. The ILP, developed by Aschoff for transfemoral amputees in 1999, features a cobalt-chrome "endo" stem that press-fits into the intramedullary canal and an "exo" module. The "endo" stem is coated with metal spongiosa to promote bone ingrowth [2, 8]. While porous coatings are common in arthroplasty, extensive coating can cause stress shielding and bone resorption, complicating revision surgery. The ILP's soft tissue interface has been redesigned several times, evolving from a textured to a polished, non-abrasive surface. The textured surface led to skin breakdown, while the polished surface improved tissue drainage and resolved this issue [19].

The OPL (Paramedica, Milan, Italy) is a modified version of the original ILP prosthesis, used for both transfemoral and transtibial amputees [2, 8]. Unlike the ILP, the OPL is made of titanium to better match the elastic modulus of the host bone. While maintaining the press-fit design, the OPL replaces the spongiosa metal coating with a plasma spray roughened surface

to enhance integration. For transfemoral amputations, the OPL can feature either an extramedullary or intramedullary head [20].

Both the ILP and OPL implants use a transcutaneous "dual cone" adapter to connect the intramedullary implant to the external prosthetic. This adapter is highly polished to reduce soft tissue irritation [2, 8, 21] and includes a safety pin that fails under excessive loads, preventing fractures to the surrounding bone [22, 23]. These implants exhibit a low rate of superficial infection, and 2-year clinical outcomes show increased cortical thickness around the implant, potentially protecting against periprosthetic fractures. Overall, these implants offer alternative options to the OPRA and Compress devices and may be more suitable for certain patients. However, they are not currently approved for clinical use in the United States, and there are no direct comparative studies of the various transdermal orthopaedic implants. Future research is necessary to determine the most appropriate implants for specific amputee populations.

1.3. Challenges of Osseointegration

Complications in the use of transcutaneous implants are frequent due to underlying mechanisms that inhibit achieving a proper bond between the implant and the soft tissues around. The primary cause of this is epithelial downgrowth, when epithelial cells migrate downward along the sides of the implant (Figure 3a). As this is a transcutaneous implant, closure of wound edges is not achievable, which hinders the attachment of epithelial cells to each other in a typical manner that is usually seen in wound healing. Without contact inhibition to stop cell migration, epithelial downgrowth ensues [24].

This failure of the epithelium to adhere to the implant surface leaves a gap at the skin implant interface, creating a direct path for microorganisms to access the underlying tissues. Marsupialization, a process where pockets form between the implant and the surrounding epithelium because of epithelial downgrowth, is depicted in Figure 3b. These pockets accumulate cell debris and exudate, creating an ideal environment for bacterial colonization [24].

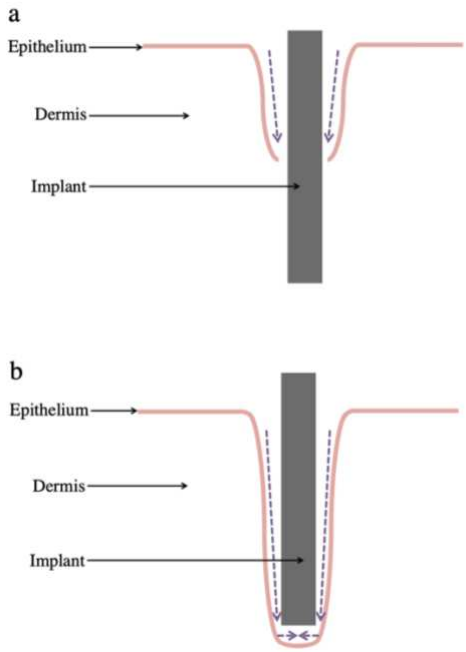

Figure 3 - Diagram depicting the process of (a) epithelial downgrowth and (b) marsupialization [24].

Regardless of the design or surgical approach, all osseointegration implants experience the same obstacles, with transdermal implants being the most affected by infections. The predominant infective pathogens in these instances include, but are not limited to, *staphylococcus aureus* and coagulase negative *staphylococci* species. Infections typically occur at the interface between the skin and the implant, presenting symptoms such as pain, redness, and discharge. Approximately half of OI patients experience superficial infections, which are generally resolved with antibiotics and rarely progress to affect the underlying bone. Nevertheless, even though they are less common, deep infections are more often problematic clinically as they may result in factors such as loosening of the implant, the need for further surgical procedures, or in some instances, the total removal of the implant [4].

Numerous approaches have been suggested to mitigate the dangers and effects of infections associated with osseointegrated implants. One approach involves rigorous wound monitoring protocols to minimize unnecessary surgical interventions for infection management. Another one focuses on enhancing the implant itself with antibiotic or silver nanoparticle coatings, which have demonstrated promising results in pre-clinical studies. However, these methods have yet to undergo testing in human subjects, leaving their actual effectiveness uncertain. As a result, exploring alternative methods for preventing and treating infections remains essential [4].

1.4. Strategies to Address Soft Tissue Integration

The effectiveness of osseointegrated transcutaneous prostheses relies on forming a soft-tissue seal at the skin-implant junction to prevent infections.

In an older study by Pendegrass, C. J., *et al.* (2008), the proliferation, morphology, and attachment of keratinocytes to four titanium-alloy surfaces were evaluated to identify the optimal topography *in vitro*. Immunolocalization of adhesion complex components, scanning electron microscopy, and transmission electron microscopy were employed to assess cell parameters. It was demonstrated that the surface topography of biomaterials significantly influences the proliferation, morphology, and attachment of keratinocytes. Smoother surfaces were found to enhance adhesion. It is hypothesized that maintaining a smooth topography at the epithelium-ITAP interface could enhance attachment *in vivo*, thereby creating an effective barrier against infection [39].

In another older study by Pitkin, M. *et al.* (2006), cell adhesion and penetration of osteocytes, fibroblasts, and keratinocytes into the pores of a porous titanium pylon implanted in the residual thigh bone of Wistar rats were investigated. Electron scanning and morphological analysis revealed integration of the pylon with the surrounding skin. These findings suggest the potential to develop a natural barrier against infections associated with direct skeletal attachment of limb prostheses [40].

A series of studies by Chimutengwende-Gordon M. *et al.* explored the integration of soft tissue into porous titanium alloy structures.

The first study (Chimutengwende-Gordon, M. *et al.*, 2018), investigated how different pore and strut sizes affect soft-tissue growth in fully porous titanium alloys. The hypothesis was that implants with a more open porous structure and larger pore sizes would promote soft-tissue ingrowth. Porous titanium alloy cylinders were implanted into the paraspinal muscles of sheep (n = 6) and left in place for four weeks. Histological assessments of soft-tissue ingrowth were conducted, quantifying the percentage of soft-tissue pore fill, cell nuclei density, and blood vessel density. The findings indicated that larger pore sizes favoured tissue integration with a structure featuring 700 μm pores and 300 μm struts showing the most successful revascularization [35].

In another study, Chimutengwende-Gordon M. *et al.* (2011) aimed to improve *in vitro* fibroblast adhesion to silanized fibronectin (SiFn) on titanium alloy by omitting the passivation stage. Additionally, it evaluated the effects of SiFn on *in vivo* dermal attachment, comparing these results with those from adsorbed fibronectin (Fn), hydroxyapatite (HA), Fn adsorbed onto

HA (HAFn), and uncoated controls. Surface topography was analysed using scanning electron microscopy, profilometry, and contact angle measurements. Anti-vinculin antibodies were utilised to immunolocalize fibroblast adhesion sites. Histological assessments of soft-tissue attachment and cell alignment relative to implants were conducted in an *in vivo* ovine model. Passivation produced rougher, more hydrophobic, and microcracked surfaces, which correlated with poorer fibroblast adhesion compared to unpassivated controls. SiFn and HAFn surfaces showed improved cell alignment *in vivo*, suggesting enhanced dermal attachment. These findings imply that SiFn and HAFn surfaces could be beneficial for optimizing the soft tissue seals around ITAP implants [36].

A third study (Chimutengwende-Gordon, M. *et al.*, 2017) examined the role of ITAP pins featuring a fully porous titanium alloy flange with interconnected pores on soft-tissue integration. The flanges were coated with fibronectin-functionalized hydroxyapatite and silver coatings, known for their antibacterial properties and ability to promote viable fibroblast growth *in vitro*. The ITAP pins were implanted along the length of ovine tibias, and a histological assessment was performed four weeks post-operatively. The porous titanium alloy flange demonstrated a reduction in epithelial downgrowth and an increase in soft-tissue integration when compared to the standard drilled flange. However, additional coatings, including fibronectin-functionalized hydroxyapatite and silver coatings, did not further enhance these effects. This suggests that a fully porous titanium could improve the soft-tissue seal around ITAP, reducing the risk of infection [37].

A more recent study by Wang, X. *et al.* (2021) investigated surface modification to enhance biological sealing. In this study, Ti–6Al–4V titanium alloy sheets and screws were modified with fibrinogen (Ti-Fg), polydopamine (PDA) or a combination of both (Ti–PDA–Fg). The modified surfaces showed significantly better adhesion and spreading of key cells, including human epidermal keratinocytes (HaCaT), human foreskin fibroblasts (HFF), and preosteoblasts (MC3T3-E1), compared to unmodified titanium. *In vivo* tests on rats demonstrated that the Ti–PDA–Fg combination attenuated soft-tissue responses and promoted angiogenesis after subcutaneous implantation. Furthermore, in a percutaneous tibial implantation model, Ti–PDA–Fg screws significantly inhibited epithelial downgrowth and promoted new bone formation. These results suggest that PDA and fibrinogen coatings hold promise for enhancing the biological sealing and osseointegration, with both soft and hard tissues, which is critical for success of orthopaedic percutaneous devices [38].

Despite several attempts to improve soft tissue-prosthesis integration, there are no long-term *in vivo* studies demonstrating its effectiveness. Similar animal experiments were tried by

Holt, B. M. *et al.* (2013), using a subdermal barrier system which was coated with a 500–750 μm thick commercially pure titanium porous coating (p2 type, DJO Global, Austin, TX) with a porosity of 52 + 12%, providing an initial mechanical and biological protection against infection. However, persistent epithelial down growth eventually compromised the attachment over a two-year period. This indicates that a permanent sealed skin/implant interface and complete wound healing were not still achieved [41].

1.5. Aim and Objectives of the Work

The objective of this work is to explore innovative ways to enhance the soft tissue integration with transcutaneous osseointegrated prostheses at the lower limb. These prostheses employ a titanium alloy-based implant that is infixed in the bone (osseointegrated) and protrudes through the skin (transcutaneous) to allow direct skeletal attachment of the artificial limbs to the bone.

Even though the osseointegration process does a very good job of anchoring the implant into the bone, the major problems are faced at the stoma, the point where the implant passes through the skin. This is a common area for infections and in extreme cases, the implant must be removed. Additionally, during the early stages of rehabilitation, fibrotic soft tissue with exudate often adheres to the abutment, the component connecting the fixture to the prosthetic limb, causing painful “tearing” of tissues. Even with the stabilization of the stoma enclosing the implant, soft tissue movement over the abutment can cause irritation, which can progress to inflammation.

In order to tackle these challenges, a comprehensive and multi-dimensional perspective is essential. This dissertation proposes a bioactive coating for abutments, which is purposefully designed to interface with soft tissues and to promote their vascularization.

Soft tissue regeneration is facilitated by effective angiogenesis to provide necessary nutrients and oxygen. Vascular regeneration has been enhanced by several growth factors including VEGF, PDGF and bFGF. On the other hand, their high price and short half-lives considerably dampen their efficacy. Metal ions, such as copper, zinc, and cobalt, are known to stimulate angiogenesis by different means. Copper ions, for instance, increase the secretion of vascular endothelial growth factor (VEGF) which is imperative for the growth of new blood vessels. Use of metal ions is also associated with some drawbacks such as cytotoxicity and oxidative stress when used in high concentrations as well as health concerns from their buildup in the body.

L-Arg, an essential α-amino acid, has found its applications in preparations for biomaterials primarily due to its good biocompatibility, various physiological advantages, and low price. L-Arg is converted by nitric oxide synthase (NOS) and arginase to the corresponding metabolites, ie. NO and ornithine, respectively. In addition, NO induces the release of VEGF, a factor critical to angiogenesis, whereas ornithine is a source of proline, which is involved in collagen production.

Gelatin is a natural polymer derived from protein, cointaining bioactive peptides such as arginine, which assists in cell adhesion. But its usage in scaffold development has some drawbacks, such as lesser mechanical properties and quicker degradation with the enzyme action. To address these limitations, this work synthesized GelMA to improve its mechanical properties and stability. GelMA-based scaffolds were produced using the cryopolymerization method. Additionally, the incorporation of other polymers was investigated to identify a suitable system for soft tissue engineering. Specifically, blends with methacrylated chitosan, pectin hydrogel, and a branched polymer such as PEGDA 4-arm were assessed.

Cryopolymerization was chosen as the fabrication method. This process creates cryogels through an ice-templating technique at sub-freezing temperatures. Compared to traditional hydrogels, cryogels demonstrate superior mechanical strength, featuring a macroporous structure and excellent pore connectivity that closely resemble the architecture of natural soft tissues. The interconnected porous network promotes efficient nutrient transport and offers ample space for cell adhesion and proliferation.

2. Materials and Methods

2.1. Materials

2.1.1. Standards

All standards and reagents, including low-molecular-weight chitosan and gelatin from porcine skin, were obtained from Sigma Aldrich (Milan, Italy), unless specified otherwise.

2.1.2. Low-molecular-weight Chitosan

Chitosan is a linear polysaccharide consisting of randomly distributed β-(1→4)-linked D-glucosamine (deacetylated units) and N-acetyl-D-glucosamine (acetylated units). It is produced by treating chitin with an alkaline substance like sodium hydroxide [42]. Chitosan has a wide array of commercial and possible biomedical uses and, due to its cationic nature, its biocompatibility and biodegradability and also non-toxicity and adsorption properties, has been recognized as a functional biopolymer [43].

2.1.3. Gelatin from Porcine Skin

Gelatin derived from porcine skin is produced through the acidic digestion of collagen and is known as type A. It primarily consists of glycine, proline, and hydroxyproline. Following digestion, gelatin adopts a random coil structure, unlike the triple helical structure of collagen. It differs from type B bovine gelatin in its N-terminal sequence. Gelatin has been utilized in various applications, including the creation of scaffolds for tissue engineering purposes.

2.1.4. Pectin

Pectin, as other complex polysaccharides, is formed by three interrelated domains: homogalacturonan, rhamnogalacturonan I, and rhamnogalacturonan II. The primary characteristic of pectin is a linear sequence of α-(1,4)-linked D-galacturonic acid units, known as the homogalacturonan domain or the "smooth region" of pectin. Another feature of pectin's structure is the regular presence of rhamnose sugars. The sequence of α-(1,4)-linked D-galacturonopyranosyl units can be interrupted by the inclusion of α-(1,2)-linked L-rhamnopyranosyl units, resulting in rhamnogalacturonan I, which typically has sidechains containing arabinose and galactose. Finally, there is rhamnogalacturonan II which is the least abundant but is also important in the structure of pectin where it is present as an extensively branched oligosaccharide analogue of homogalcturonan [44].

2.1.5. PEGDA

As a derivative of polyethylene glycol, PEGDA is an important biocompatible and biodegradable environmentally friendly polymer material. It can use a certain amount of initiator to initiate polymerization under heating, light and radiation conditions. PEGDA has low viscosity, low volatilization and fast curing properties, and can be used in plastic coatings, metal coatings, offset inks, flexography, and screen printing, polymer coatings, and biomedical fields.

2.2. Methods

2.2.1. Methacrylation Reaction

Methacrylation refers to the process of adding a methacrylate group to a molecule. This group contains a double bond between a carbon and an oxygen atom, with a methyl group attached to the carbon atom. Methacrylate groups are often used in the production of polymers and hydrogels which have many applications, especially in tissue engineering and drug delivery [45].

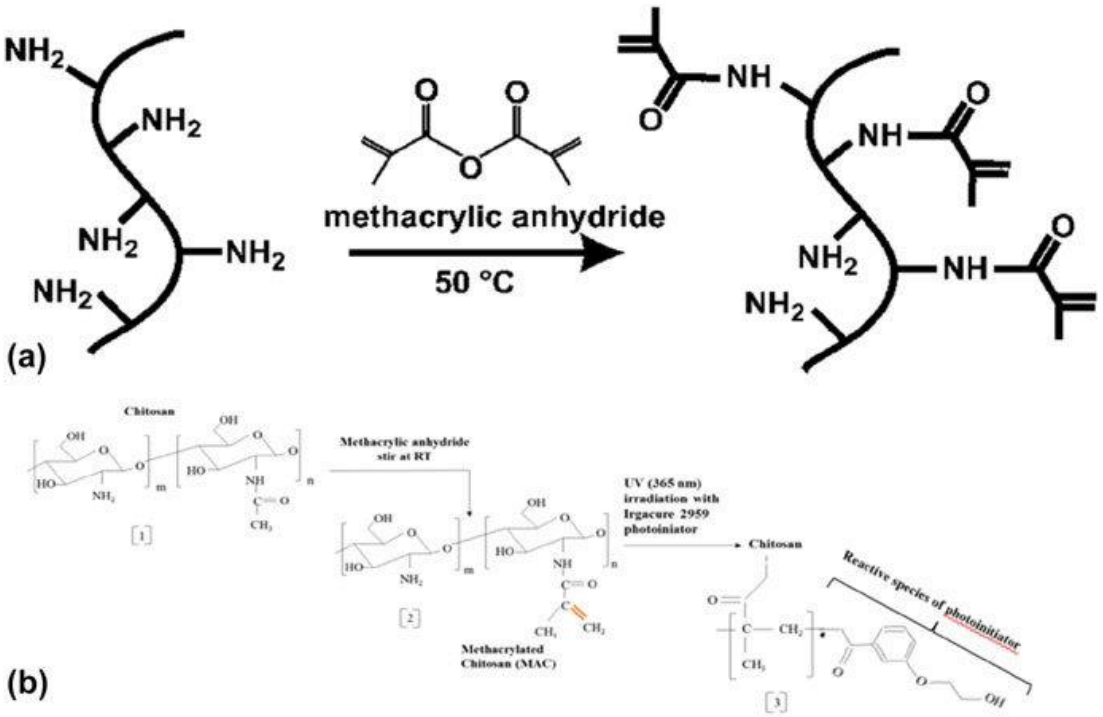

Figure 4 - Methacrylation Reaction for (a) gelatin and for (b) chitosan [46].

2.2.1.1. Gelatin Methacrylation Procedure

Briefly, 10 g of Gelatin from porcine skin (type A, Sigma Aldrich, Milan, Italy) was dissolved into 100 ml of PBS at 50 °C. Next, 1.4 ml of methacrylic anhydride (MW: 154.16 g / mol, # 276685, Sigma Aldrich, Milan, Italy) was added dropwise to the solution and stirred for 3h at 50 °C. After 3 hours, 400 ml of preheated PBS were added, and the resulting solution was kept at 50 °C for 15 min.

Figure 5 - GelMA synthesis.

Unreacted methacrylic anhydride and by-products were removed by dialysis against distillated water for 8 days using Spectro/Por molecular porous membrane tubes (MWCO 12-14.000, # 08-801-244, Fisher Scientific, Milan, Italy). Then, GelMA50 solution was frozen at -80 °C into 50 ml falcon tube, for at least 2 days and then lyophilized and stored at −20 °C.

Figure 6 – GelMA dialysis.

2.2.1.2. Chitosan Methacrylation Procedure

Briefly, 0.75 g of low-molecular-weight chitosan was dissolved in 50 mL of a 1M aqueous acetic acid solution at 50°C and, subsequently, stirred until a homogeneous solution is achieved. Next, 500 μL of MA was added dropwise until reaching a molar ratio of 0.79:1 (MA:CH) to achieve 30% methacrylation [52]. The reaction temperature was maintained at 50°C and the solution was stirred constantly for 4 hours. Then, 250 ml of PBS were added, and the resulting solution was kept at 50 °C for 15 min. The reaction mixture was then dialyzed against distilled water for 4 days to remove unreacted reagents and by-products. After dialysis, the product was freeze-dried to obtain the methacrylate chitosan. The freeze-drying process is carried out under vacuum to remove water without causing degradation of the product.

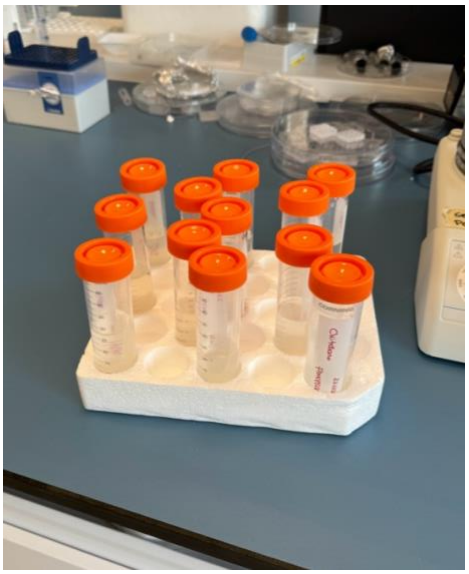

Figure 7 - Chitosan solutions in falcon tubes, before freeze-drying.

2.2.2. Cryogel Preparation

2.2.2.1. Cryopolymerization

The polymerization of water-soluble monomers under frozen conditions, known as cryopolymerization, has been widely utilised to create multifunctional macroporous cryogels, commonly referred to as cryogels. Compared to other pore-forming methods, freezing offers significant flexibility in designing pore architecture. Pore morphology can be easily adjusted by varying freezing conditions such as precursor viscosity, freezing temperatures, solution concentrations, and cooling rates. High aspect ratio-oriented pore structures, which are challenging to achieve with other techniques, can be readily obtained through unidirectional freezing (UF). Additionally, organo-phase cryogelation of linear polymers and cryopolymerization of oily monomers have been developed to synthesize non-water swellable polymer foams [47].

Cryopolymerization of gelatin methacrylate produces CryoGelMA, a cryogelation product derived from existing GelMA. Cryogelation is an affordable and straightforward method for creating macropores that can house biomolecules, such as growth factors. Besides the inherent benefits of GelMA, CryoGelMA can accommodate higher concentrations of biomolecules compared to GelMA [48].

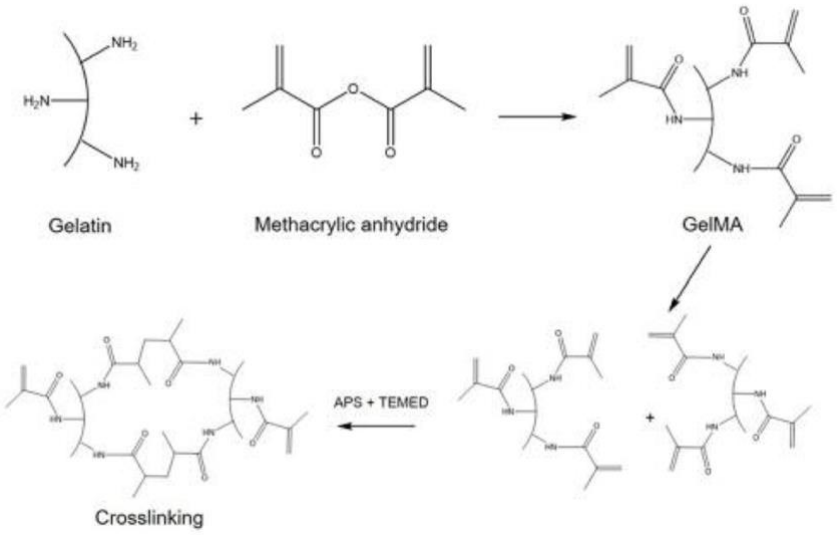

Figure 8 - Cryopolymerization of GelMA [49].

2.2.2.1.1. Cryopolymerization of GelMA

Cryopolymerization of GelMA (4% w/v) + Pectin (2% w/v) or PEGDA (0.5%, 1%) through thawing (-20°C for 72h) and washing cycles (1,2,3…), washing in PBS prior to use, using APS as the initiator agent (2% w/v) and TEMED as a catalyst (1%) [56].

Figure 9 – Cryogels after thawing.

2.2.2.2. Free Radical Polymerization

At the same time as cryopolymerization, GelMA and CsMA were crosslinked using UV light with LAP as a photoinitiator, as further confirmation of successful methacrylation in addition to the IR and ninhydrin assay.

During the cross-linked free radical polymerization reaction, oligomers and monomers that are functionalized with carbon–carbon double bonds react to form single covalent bonds, creating a three-dimensional cross-linked polymer network. The free radicals necessary for this reaction are generated by photoinitiators [50].

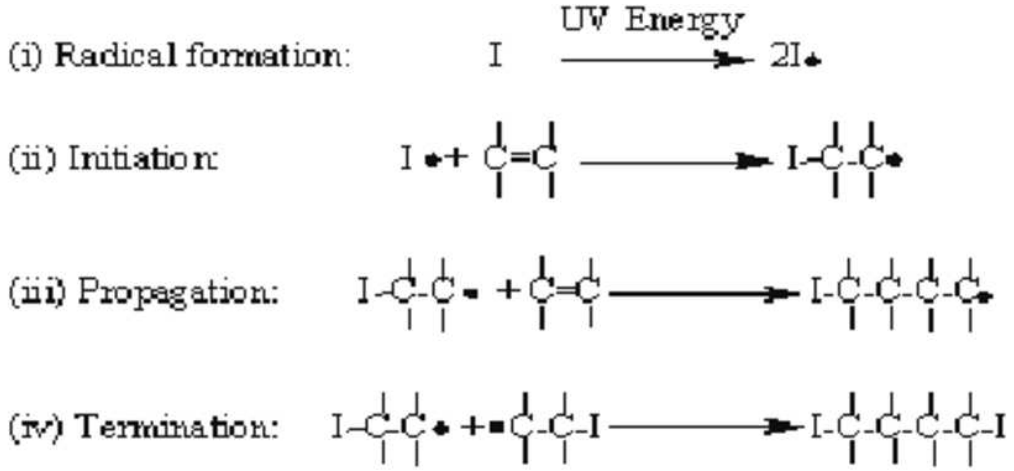

Figure 10 - UV free radical polymerization process [51].

The photo-initiator (I) absorbs light and forms a radical species (Ix). During the initiation step, this radical species reacts with the carbon double bonds (-C=C-) of the acrylate groups in the oligomer. In the propagation step, the reactive species continue to react with additional acrylates, forming new radicals and perpetuating the polymerization process. The process is terminated when two growing oligomer chains react with each other, as depicted in Figure 10 [51].

2.2.2.2.1. UV Polymerization

Solutions of GelMA (10% w/v in 10% FBS and 90% PBS solution) and CsMA (1.5% and 3% w/v in 2% v/v acetic acid solution) were prepared at 40 ˚C with agitation. Then, 0.5% w/v of LAP (MW: 294.21, Sigma Aldrich, Milan, Italy) was added as a photo-initiator, and stirred at 40˚ C for 1h. Consequently, the solutions were separated into portions and poured into a silicon mold. They were then placed under UV light with a wavelength of 365 nm for a period of 2 minutes to facilitate the formation of crosslinked hydrogel constructs [57].

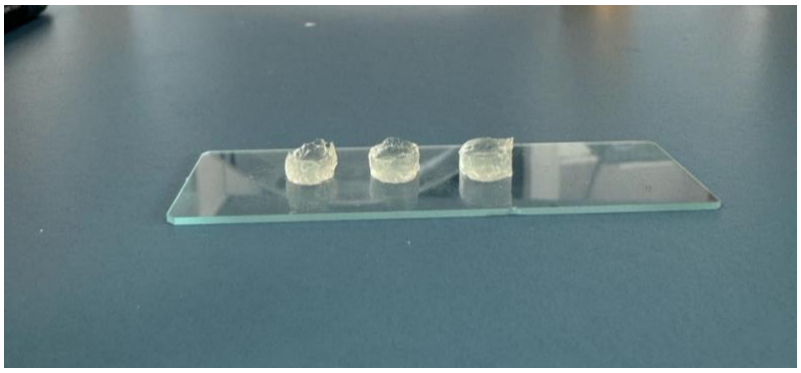

Figure 11 - Hydrogel with 10% GelMA, after UV polymerization.

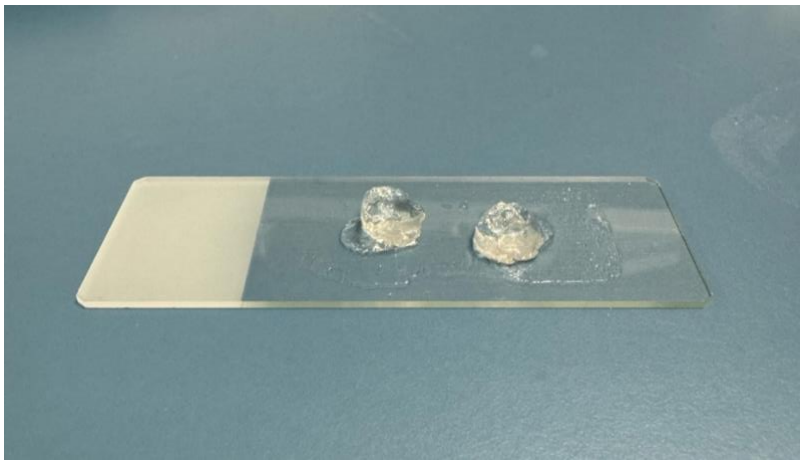

Figure 12 - Hydrogel with 1.5% w/v CsMA, after UV polymerization.

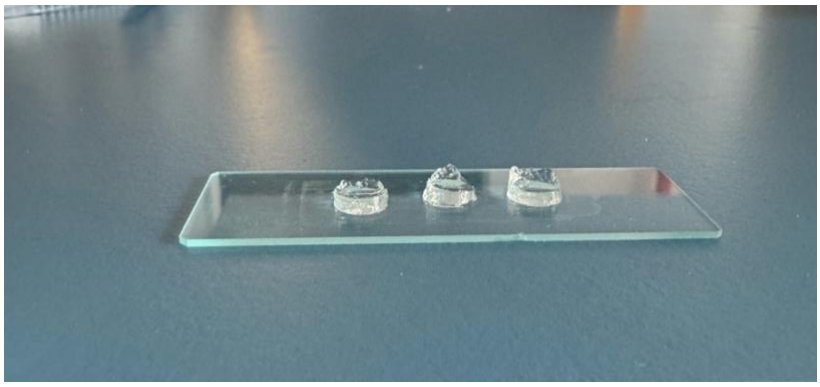

Figures 13 - Hydrogel with 3% w/v CsMA, after UV polymerization.

2.2.3. Chemical Characterization

2.2.3.1. Fourier-Transform Infrared (FTIR) Spectroscopy Test

Fourier Transform Infrared Spectroscopy is a technique for material identification that is used with organic compounds, polymers and sometimes inorganic materials as well. It consists of analysing the chemical properties of samples by exposing them to infrared rays.

The FTIR device transmits infrared light within the range of about 10,000 to 100 cm^{-1} through a certain sample. A part of this radiation is absorbed by the sample and the remainder goes through it. The absorbed radiation causes the sample molecules to increase in rotational and/or vibrational energy. The end signal, in which the course of the sample absorption in the given range appears as a spectrum, is usually in the range of 4000 cm^{-1} to 400 cm^{-1}.This spectrum acts as a molecular fingerprint unique to each molecule or chemical structure, making FTIR analysis a highly effective tool for chemical identification.

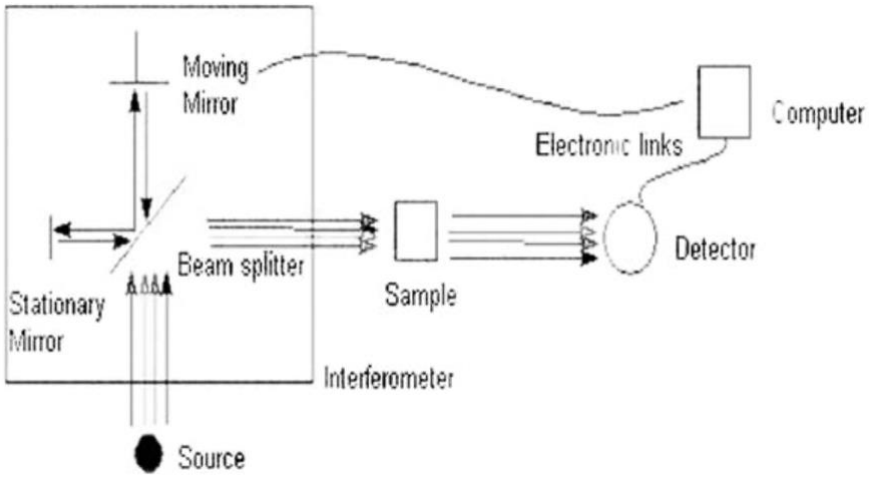

Figure 14 - Schematic diagram of a Fourier transform infrared instrument [53].

IR spectra can be obtained from samples in various phases, including liquid, solid, or gas. For solid samples, one common method involves grinding the sample with potassium bromide (KBr) to form a fine powder. This mixture is then pressed into a thin pellet or disk, which is placed in the path of the infrared light beam during the measurement. This preparation allows for the analysis of the sample's infrared absorption characteristics [53].

In this work, samples of gelatin and chitosan, both modified and unmodified, were analysed using an FT/IR – 6300 type A spectrometer scanning from 600 to 4000 cm^{-1} with a resolution of 4 cm^{-1}. FTIR spectra were acquired to analyse the molecular interactions and identify the functional groups of GelMA and CsMA. Pure gelatin and pure chitosan, and synthesised GelMA and CsMA hydrogel and KBr were mixed in a ratio of 1:100, and FTIR analysis was implemented after tableting.

2.2.3.2. Ninhydrin assay

The ninhydrin test is a chemical assay used to detect ammonia, primary and secondary amines, or amino acids. In samples with these groups, the addition of ninhydrin reagent

produces a very intense deep blue coloration termed as Ruhemann's purple, which denotes the presence of amino group.

When ninhydrin (2,2-dihydroxyindane-1,3-dione) is applied on an amino acid, oxidative deamination of the amino acid occurs and carbon dioxide, ammonia and an aldehyde are released, resulting in the substance hydrindantin. The ammonia produced will then interact with another ninhydrin producing a compound called diketo hydrin, commonly known as Ruhemann's complex.

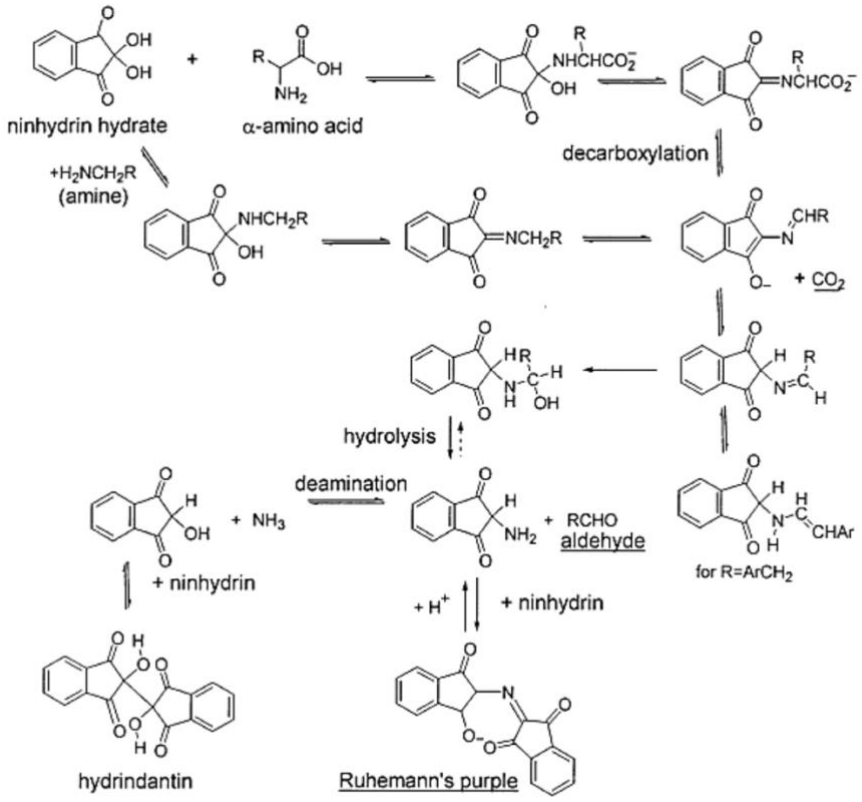

Figure 15 – Mechanisms of reactions of α-amino acids, amines, and trifunctional amino acids with ninhydrin hydrate to form Ruhemann's purple and other products [54].

A positive ninhydrin test is understood where a purple-coloured complex appears within the test tube confirming the presence of an amino acid within the sample. In the absence of such change in colour with the resulting complex being purple in colour, the test is therefore negative meaning no amino acids are present in the sample.

In this work, a 2% w/v ninhydrin solution in DMSO was prepared by stirring for 12 hours at room temperature in the absence of light. Solutions of unmodified and modified chitosan ranging from 0.05% to 0.5% w/v were made through serial dilution, by dissolving the most concentrated one in 1 M acetic acid and stirring for 18 hours in the dark at room

temperature. Each polymer solution (0.5 mL) was mixed with 5 mL of ninhydrin solution and 1.25 mL of 4 M phosphate buffer (pH 5.4 ± 0.2). These mixtures were then incubated in a water bath at 85 °C, shaken at 60 rpm for 30 minutes. Analysis was performed by measuring the absorbance at 500 using a spectrophotometer. The average absorbance for each standard was plotted to generate standard curves for both unmodified and modified chitosan. The degree of methacrylation (DoM) in percentage was calculated as: $\text{DoM}\ (\%) = 100 \times \left(1 - \frac{\text{Slope CsMA}}{\text{Slope Cs}}\right)$ [55].

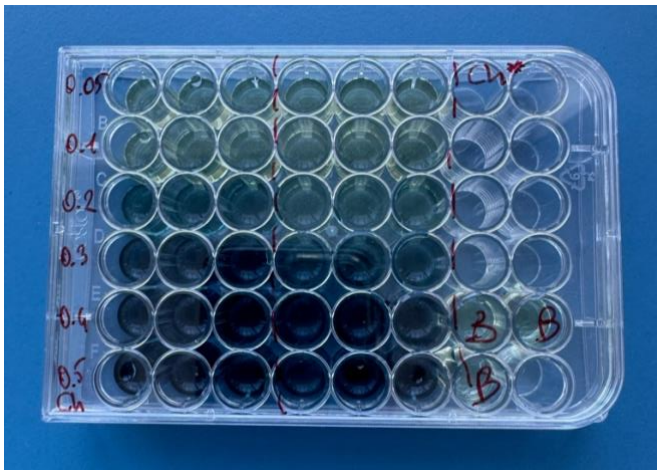

Figure 16 – Solutions ready for absorbance measurement.

GelMA samples were dissolved at a concentration of 10 mg/mL in 1x PBS. To create a standard curve, unmodified gelatin was serially diluted in PBS from 0 to 10 mg/mL in increments of 1 mg/mL and plated in triplicate in a 96-well plate. The functionalized gelatin samples were also plated in triplicate without any dilution. A 54.5 mM (10 mg/mL) solution of ninhydrin in ethanol was added to each plated sample in a 1:8 volume ratio of ninhydrin to gelatin solution, resulting in a total volume of 100 µL per well. The plate was sealed with optical sealing tape (ThermoFisher) and incubated in an oven at 100°C until a linear color development pattern was observed, which took approximately 20 minutes. Absorbance was measured at 570 nm. The average absorbance for each gelatin standard was plotted to generate a standard curve. For each functionalized sample, the fraction of available amines was determined using the following formula: $\text{Fraction of amines available} = \frac{\text{Apparent sample concentration}}{\text{Nominal sample concentration}}$, where the apparent concentration was obtained by comparison to the standard curve, while the nominal concentration was the concentration at which the protein sample solution was prepared. The degree of functionalization (DoF) in percentage [55] was calculated as:

$$\text{DoF}\ (\%) = 100 \times (1 - \frac{\text{Apparent sample concentration}}{\text{Nominal sample concentration}}) \quad .$$

2.2.4. Physical Characterization

2.2.4.1. Equilibrium Swelling Measurements and *In Vitro* Stability

The swelling capacity of a polymer, which depends on its ability to absorb liquid, provides insight into the polymer's degree of cross-linking; higher cross-linking typically reduces swelling due to retraction forces limiting chain expansion. In neutral polymers, this balance between expansion and retraction forces reaches equilibrium in a solvent at specific temperatures. Polyelectrolyte polymers, such as chitosan, experience additional swelling due to fixed charges that attract more water, known as the "Gibbs-Donnan effect." This property is crucial for drug-controlled-release systems, as increased membrane swelling enhances diffusivity, allowing larger molecules to pass through, thereby playing a vital role in the transport of cells and growth factors through membranes.

In this work, dry cryogel discs are used for equilibrium swelling measurements in PBS at 37°C. Samples are frozen at -20ºC, lyophilized overnight and weighed at predetermined time points (within 24 hours). Swollen samples are removed from PBS, gently blotted to remove excess PBS, and then weighed. The equilibrium swelling ratio is calculated using the formula: $\text{Swelling Ratio}\ (\%) = (W_{wet} - W_{dry})/W_{dry} \times 100$, where W_{wet} is the weight after hydration in PBS and W_{dry} represents the initial dry weight of the hydrogel/cryogel [58].

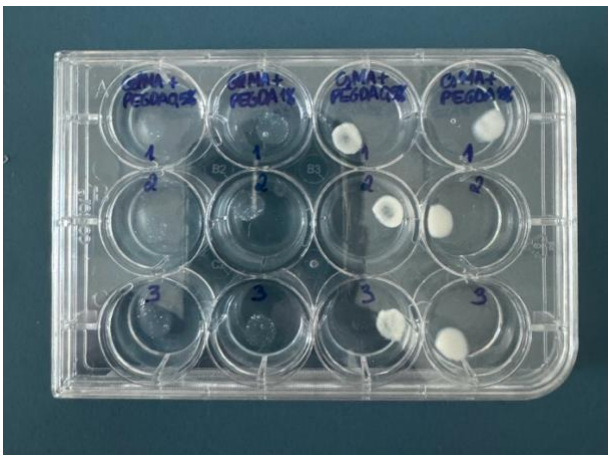

Figure 17 - GelMA and CsMA cryogels with PEGDA (0.5%, 1%) during swelling test.

In this work, the stability of the cryogel was assessed by observing its non-enzymatic degradation. Initially, samples were weighed (t = 0). Subsequently, the weight was monitored at various time intervals during incubation at 37°C in PBS. The GelMA samples were added 0.2% (v/v) Normocin™, an antibiotic formulation designed to prevent cell lines from mycoplasma, bacterial and fungal contaminations. The percentage of weight loss was determined using the formula: $\text{Weight Loss}\ (\%) = (W_0 - W_i)/W_0 \times 100$, which compares

the initial weight of the hydrogel/cryogel (W_0) with its weight (W_i) after hydration in PBS at 37°C at different time points [58].

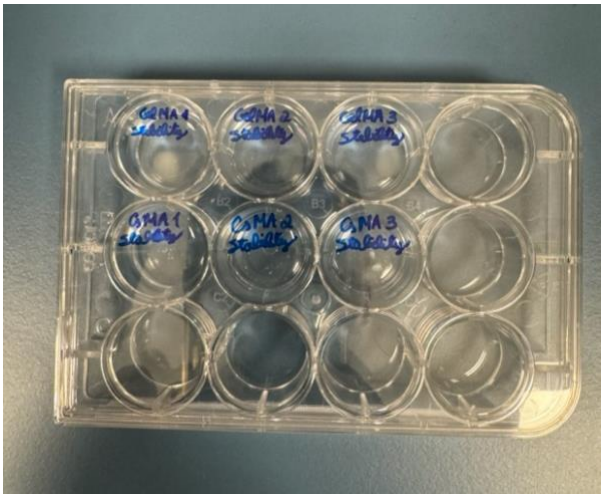

Figure 18 - GelMA and CsMA hydrogels during *in vitro* stability test.

2.2.4.2. Surface Morphology Observation

SEM utilizes a concentrated beam of high-energy electrons to produce a range of signals from the surface of solid specimens. These electron-sample interactions provide insights into the sample's external morphology (texture), chemical composition, and the crystalline structure and orientation of the materials composing the sample. Typically, data are gathered from a selected surface area of the sample, resulting in a two-dimensional image that illustrates spatial variations in these characteristics. SEM can image areas from roughly 1 cm to 5 microns in width, with magnifications between 20X and about 30,000X and a spatial resolution of 50 to 100 nm. Additionally, SEM can perform analyses on specific points of the sample, which is particularly useful for qualitatively or semi-quantitatively identifying chemical compositions (using EDS), crystalline structures, and crystal orientations (using EBSD). The SEM's design and functionality are similar to those of the EPMA, and there is significant overlap in their capabilities.

Accelerated electrons in SEM possess significant kinetic energy, which is dissipated as various signals resulting from electron-sample interactions when the incident electrons are decelerated in the solid sample. These signals include secondary electrons (which generate SEM images), backscattered electrons (BSE), diffracted backscattered electrons (EBSD used to determine crystal structures and orientations of minerals), photons (characteristic X-rays for elemental analysis and continuum X-rays), visible light (cathodoluminescence—CL), and heat. Secondary and backscattered electrons are primarily used for imaging: secondary electrons are

ideal for revealing sample morphology and topography, while backscattered electrons are valuable for illustrating compositional contrasts in multiphase samples, enabling rapid phase discrimination. X-ray generation occurs through inelastic collisions between incident electrons and electrons in discrete orbitals (shells) of the sample's atoms. As these excited electrons return to lower energy states, they emit X-rays with fixed wavelengths corresponding to the energy differences between electron shells for each element. Consequently, characteristic X-rays are produced for each element in a mineral that is excited by the electron beam. SEM analysis is considered "non-destructive," as the X-rays generated by electron interactions do not cause volume loss in the sample, allowing for repeated analyses of the same materials.

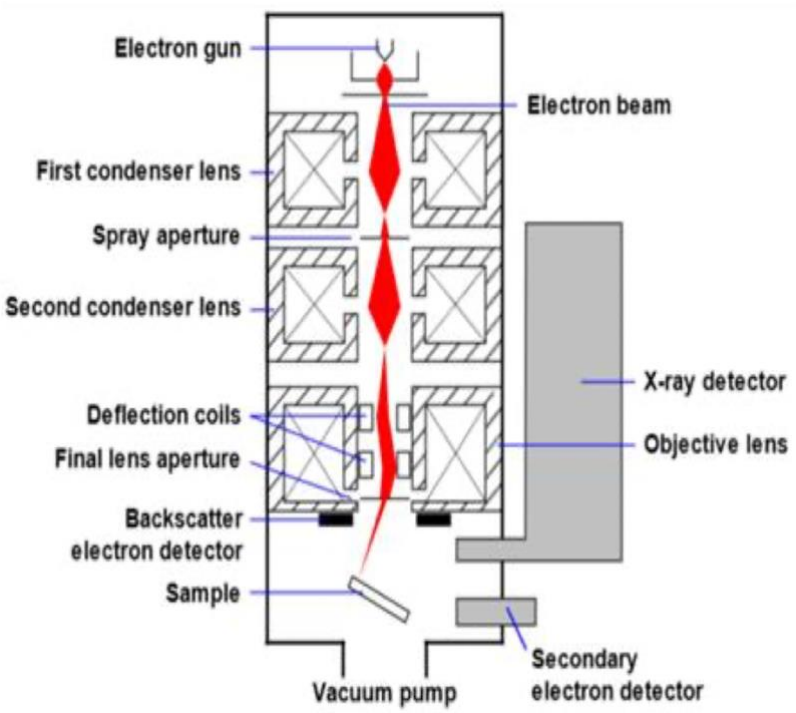

Figure 19 - Schematic of SEM [59].

In this work, cryogels were washed with deionized water to remove PBS salt. Samples are cut in the middle, lyophilized for 3 days, and sputter coated with gold for SEM imaging. The porous structure of the cryogels was observed by SEM. Measurements of the average pore sizes of the crogels are done based on SEM images.

Figure 20 - Samples being sputter coated with gold.

Figure 21 - Sigma 300 VP SEM.

2.2.5. Mechanical Testing

2.2.5.1. Rheological Characterization

Cryogels generally exhibit elastic and viscous properties depending on the conditions in which they are processed. These properties relate to the storage modulus, denoted by G', which indicates elastic behaviour, and to the loss modulus, represented by G'', which implies viscous behaviour. GelMA cryogel systems, with and without the addition of PEGDA, were subjected

to an analysis of its G' at 25 ºC and *in situ* using a rheometer (Physica MCR 301, Anton Paar) as it was being formed. The rheometer setup consisting of a two-plate configuration (plate of 25 mm diameter and 0.5 mm gap distance) was placed in a water bath circulator setup. Between the plates, the solid cryogel structure was positioned, and the storage modulus was recorded using a time sweep oscillatory test held at constant strain amplitude of 1% and a frequency of 1 Hz, which was within the range of linear viscoelastic (LVE) region. During the time sweep test, both the storage and loss moduli were recorded over a period of 15 minutes.

Figure 22 - Physica MCR 301 rheometer Anton Paar.

2.2.5.2. Compression Test

The mechanical properties of cryogels were assessed via compression mode testing, which is used to determine a material's behaviour under a compressive load, while they were in a hydrated state. Prior to testing, samples were immersed in PBS for 10 minutes. Compressive mechanical tests were performed on a Zwick testing machine connected to a 10 N load cell. Compressive tests were done by maintaining a crosshead speed of 2 mm/min until a maximum compression of 40% was maintained. The compressive modulus was calculated from the initial

slope of the stress strain curves at 10% strain. Descriptive statistics are provided as mean ± standard deviation for a sample size of three (n=3).

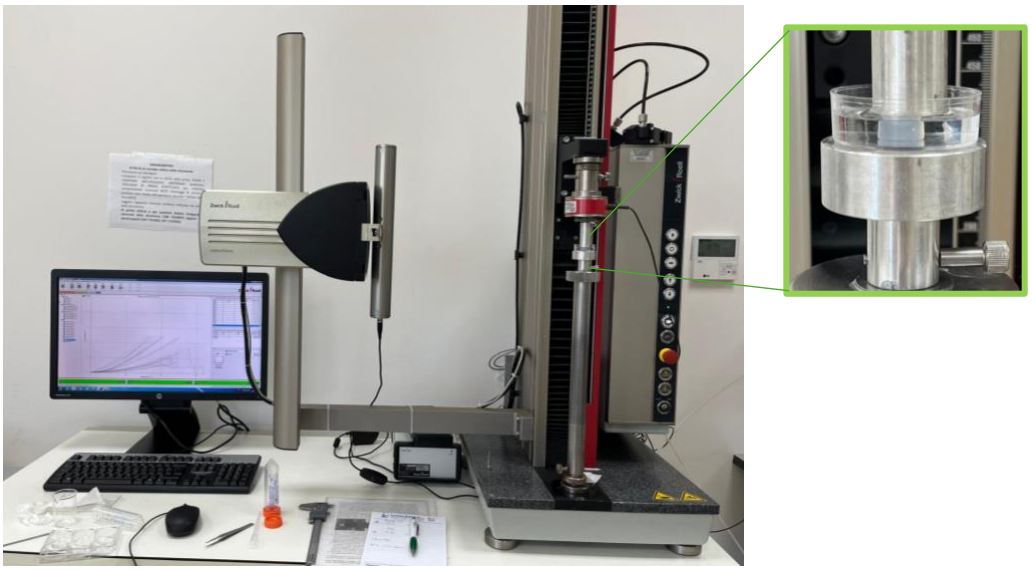

Figure 23 - Zwick universal testing machine. In the green box, there is the PVA scaffold immersed in PBS during the compression test.

2.2.5.3. Biocompatibility Test

Biocompatibility tests assess how the material interacts with biological systems to ensure that it doesn't cause adverse reactions, such as toxicity, inflammation, or immune responses

In this work, biocompatibility tests were conducted on cryogels made from GelMA, GelMA_PEGDA0.5%, and GelMA_PEGDA1%. The samples were synthesized in a 48-well plate and optimized for cell growth and viability.

At first, the cryogel samples were allowed to gradually thaw and were rinsed three times with PBS to remove excess reagents. The samples were then placed in 6-well plates with not more than three samples per well. Also, 5 mL of culture medium was provided (consisting of 90% DMEM, 10% FBS, 1% glutamine, and 1% penicillin/streptomycin mix). Following 40 minutes under UV light to sterilize the cryogels, 6×10^4 U251 glioma cells were harvested for each sample, occupying each scaffold's designed volume.

Cell viability was evaluated via the Calcein AM/PI live/dead assay method. Dyes were added to the samples consisting of 100 µL of PI (1 mg/mL in PBS), 900 µL of PBS, and 1.5 µL of Calcein (1 µg/µL in DMSO), and samples were kept for up to 7 days. Live/Dead assays were carried out on Days 1 and 7 in order to differentiate live cells from dead ones, and the respective fluorescence images were taken using an EVOS m7000 microscope. Green filters were used to

visualize live cells stained with Calcein, while red filters highlighted dead cells stained with PI, providing insight into the biocompatibility of the cryogels.

2.3. Statistical analysis

Statistical analysis was conducted using the IBM® SPSS® Statistics software (version 30.0.0 for macOS). For comparing two lines in a graph, the analysis involved a repeated measures ANOVA test for datasets with a normal distribution and homocedasticity. For comparing three or more lines in a graph, the analysis involved an ANOVA repeated measures test for datasets with a normal distribution and homocedasticity, complemented by Tukey's HSD test for post hoc analysis. For comparing the means across multiple groups, the analysis involved a one-way ANOVA for datasets with a normal distribution and homocedasticity, complemented by Tukey's HSD for post hoc analysis. Threshold for statistical significance was established at a $p<0.05$.

3. Results

3.1. Chemical Characterization

3.1.1. Fourier Transformed Infrared (FTIR) Spectroscopy Test

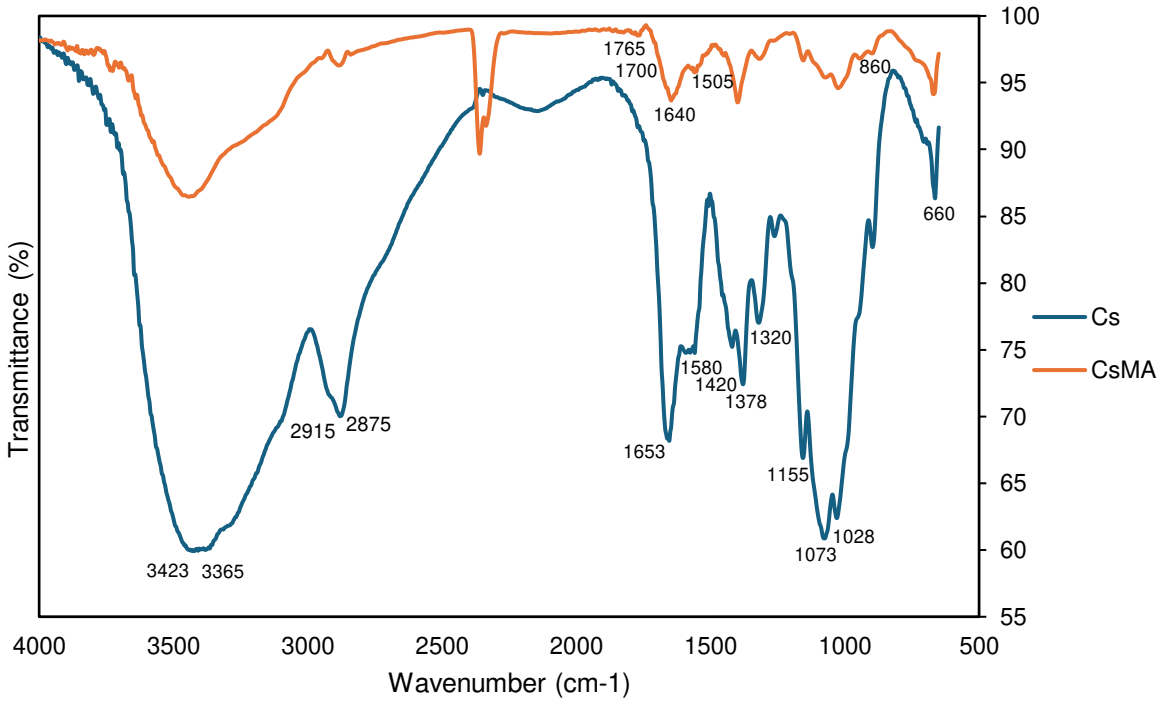

Figure 24 - FTIR spectra of Cs and CsMA.

The functional groups of both chitosan and CsMA were investigated using FTIR analysis, as illustrated in Figure 24. The Cs spectrum has a broad peak between 3365 and 3423 cm^{-1} that is due to N-H and O-H stretching and intramolecular hydrogen bonding. Another set of absorption bands situated at around 2915 and 2875 cm^{-1} is assigned to the symmetric and asymmetric stretching of the alkyl C-H groups that can be found in Cs and CsMA spectra. The bands that appear at around 1653 cm^{-1} (C=O stretching of amide I) and 1320 cm^{-1} (C-N stretching of Amide III) reflect the existence of preserved N-acetyl groups. A band at 1580 cm^{-1} suggests the bending of the primary amine N-H. The presence of CH_2 bending and CH_3 symmetrical deformations is confirmed by bands around 1420 cm^{-1} and 1378 cm^{-1}, respectively. The absorption peak located at 1155 cm^{-1} is due to the asymmetric stretching motion of the C-O-C bridge. Meanwhile, those at 1073 and 1028 cm^{-1} are associated with the C-O stretching vibrations and the one at 660 cm^{-1} corresponds to the ring stretching vibration of a pyranoside sugar. Regarding CsMA, absorption bands which appear at 1640 and 860 cm^{-1} have been

assigned to C=C double bonds created via methacrylation. The absence of N-H and O-H stretching peaks at 3430 cm^{-1}, together with new peaks appearing at 1505 and 1700 cm^{-1} labelled as C-N stretching and N-H bending, respectively, and a peak at 1765 cm^{-1} due to C=O groups, all demonstrate the anticipated changes in the chemical structure. The low intensity of these bands indicates that this degree of methacrylation in the chitosan is very limited [56, 60, 62, 63, 64].

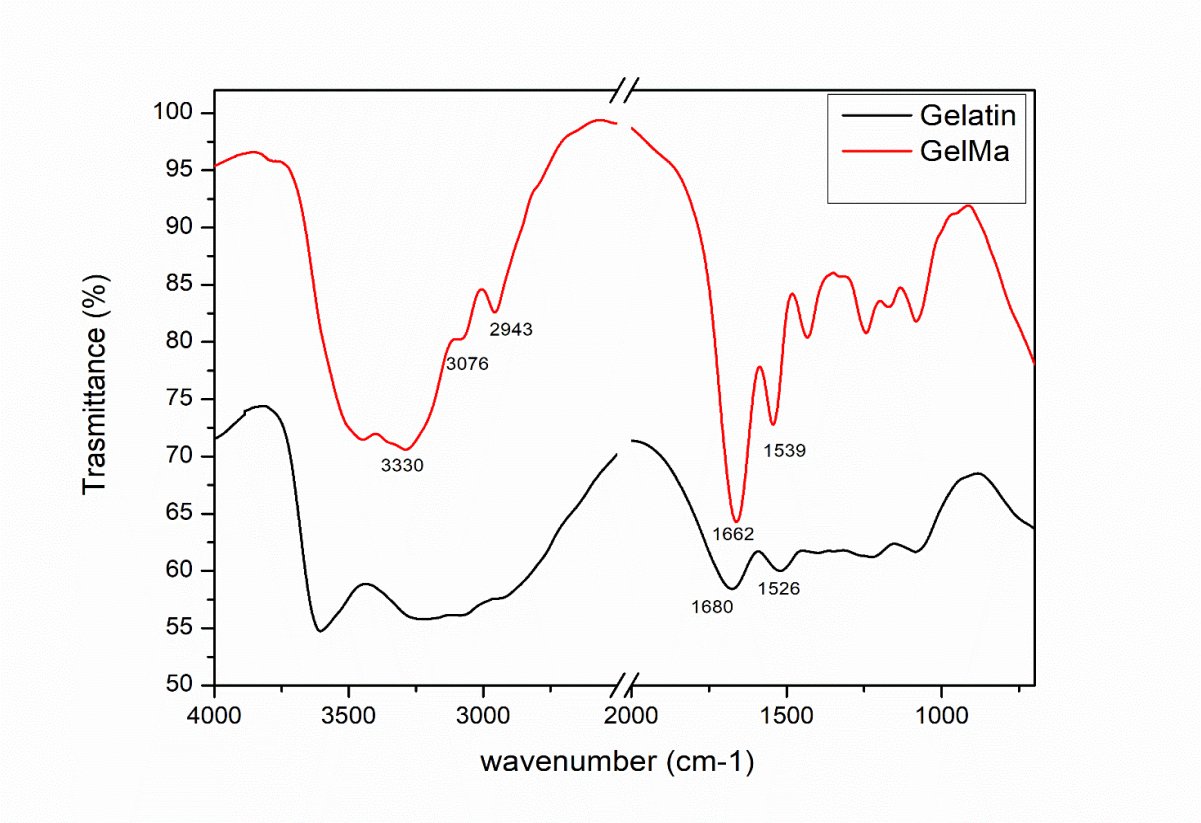

Figure 25 - FTIR spectra of Gelatin and GelMA.

The FTIR analysis, illustrated in Figure 25, was utilized to identify the functional groups present in both gelatin and GelMA. The spectra display specific vibrations at 3330 cm^{-1}, 3076 cm^{-1}, 2943 cm^{-1}, and 1662 cm^{-1}, corresponding to typical signals for O–H and N–H stretchings, N–H, saturated C–H stretching, and the amide I band, respectively [57]. In comparison to pure gelatin, the amide bands of GelMA shifted to higher frequencies. Additionally, ester and vinyl

bands may appear in the infrared spectra, confirming that the gelatin has been chemically modified to form GelMA.

3.1.2. Ninhydrin Assay

Table 1 - Absorbance at 500 nm of different concentrations of Chitosan, with the average of the measures and standard deviation.

Concentration (% w/v)	Samples Absorbance (OD)	Average Absorbance (OD)	Standard Deviation (OD)
0.50	0.651	0.743	0.150
	0.662		
	0.916		
0.40	0.464	0.523	0.055
	0.532		
	0.572		
0.30	0.366	0.413	0.041
	0.439		
	0.434		
0.20	0.212	0.230	0.016
	0.236		
	0.241		
0.10	0.094	0.104	0.009
	0.107		
	0.110		
0.05	0.078	0.075	0.003
	0.073		
	0.074		

Table 3 – Absorbance at 500 nm of different concentrations of CsMA, with the average of the measures and standard deviation.

Concentration (% w/v)	Samples absorbance (OD)	Average Absorbance (OD)	Standard Deviation (OD)
0.50	0.532	0.623	0.087
	0.630		
	0.706		
0.40	0.417	0.472	0.048
	0.494		
	0.505		
0.30	0.248	0.292	0.039
	0.324		
	0.304		
0.20	0.139	0.160	0.022
	0.182		
	0.160		
0.10	0.089	0.097	0.007
	0.100		
	0.103		
0.05	0.073	0.078	0.005
	0.078		
	0.082		

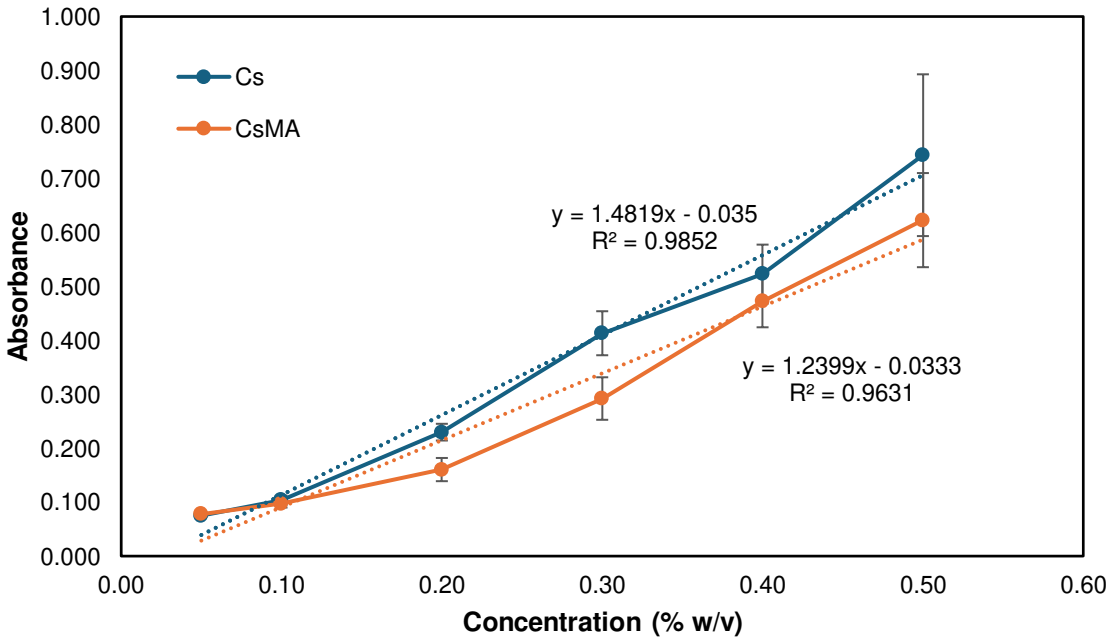

Figure 26 - Absorbance of Cs and CsMA at different concentrations.

Table 2 - Slope of the standard curves of Cs and CsMA and the degree of methacrylation.

	Slope	**Degree of Methacrylation (%)**
Cs	1.48	16%
CsMA	1.24	

Table 3 – Absorbance measurements at 570 nm of the blank and their average.

Concentration (mg/ml)	**Absorbance (OD)**	**Average Absorbance (OD)**
0	0.064	0.031
	0.009	
	0.020	

Table 4 - Absorbance at 570 nm of different concentrations of GelMA, with the blank substraction, average of the measures and standard deviation.

Concentration (mg/ml)	Samples Absorbance (OD)	Blank Subtraction (OD)	Average Absorbance (OD)	Standard Deviation (OD)
1	0.067	0.036	0.036	0.002
	0.065	0.034		
	0.068	0.037		
2	0.073	0.042	0.046	0.007
	0.073	0.042		
	0.085	0.054		
3	0.245	0.214	0.223	0.012
	0.250	0.219		
	0.268	0.237		
4	0.337	0.306	0.289	0.016
	0.316	0.285		
	0.306	0.275		
5	0.573	0.542	0.463	0.110
	0.541	0.510		
	0.369	0.338		
6	0.696	0.665	0.653	0.029
	0.704	0.673		
	0.651	0.620		
7	0.743	0.712	0.670	0.055
	0.722	0.691		
	0.639	0.608		
8	0.911	0.888	0.856	0.039
	0.908	0.877		
	0.842	0.811		
9	1.158	1.127	0.953	0.200
	1.029	0.998		
	0.765	0.734		
10	1.066	1.035	0.974	0.053
	0.976	0.945		
	0.972	0.941		

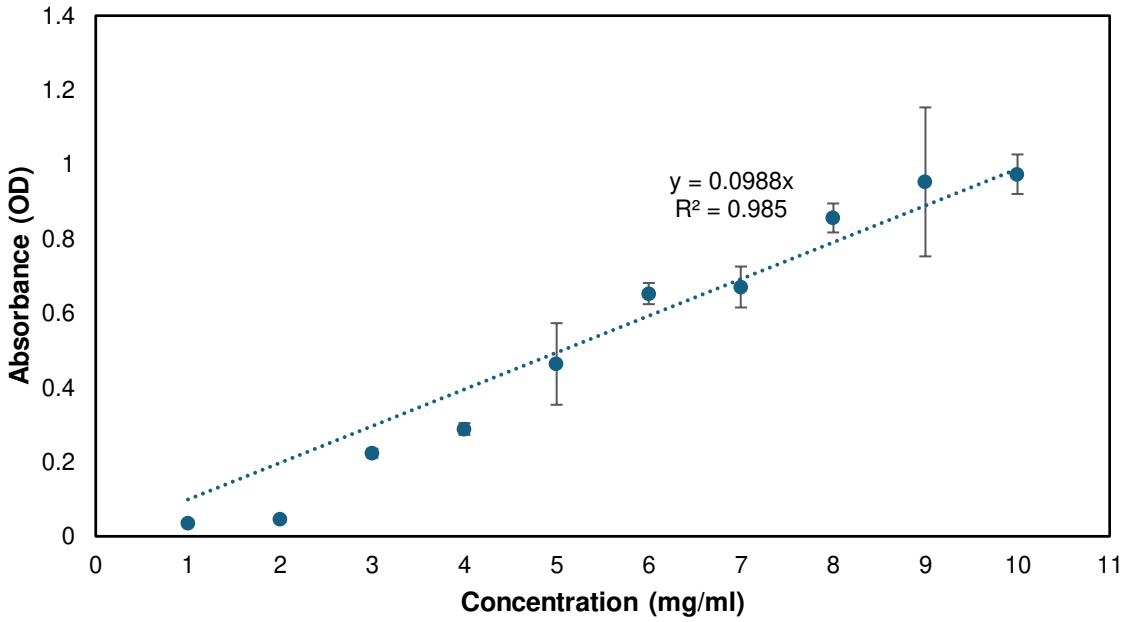

Figure 27 - Absorbance of GelMA at different concentrations.

Table 5 – Absorbance measurements, blank substraction, average of the measures, standard deviation, concentration fraction of amines available and degree of methacrylation of the sample of GelMA.

	Samples Absorbance (OD)	**Blank Subtraction (OD)**	**Average Absorbance (OD)**	**Standard Deviation (OD)**	**Concentration (mg/ml)**	**Fraction of amines available**	**Degree of Functionalization (%)**
GelMA	0.363	0.332	0.447	0.112	4.53	0.453	55%
	0.485	0.454					
	0.587	0.556					

The ninhydrin tests indicate that the degree of methacrylation of CsMA was approximately 16%, while the degree of functionalization of GelMA was roughly 55%.

3.2. Physical Characterization

3.2.1. Equilibrium Swelling Measurements and *In Vitro* Stability

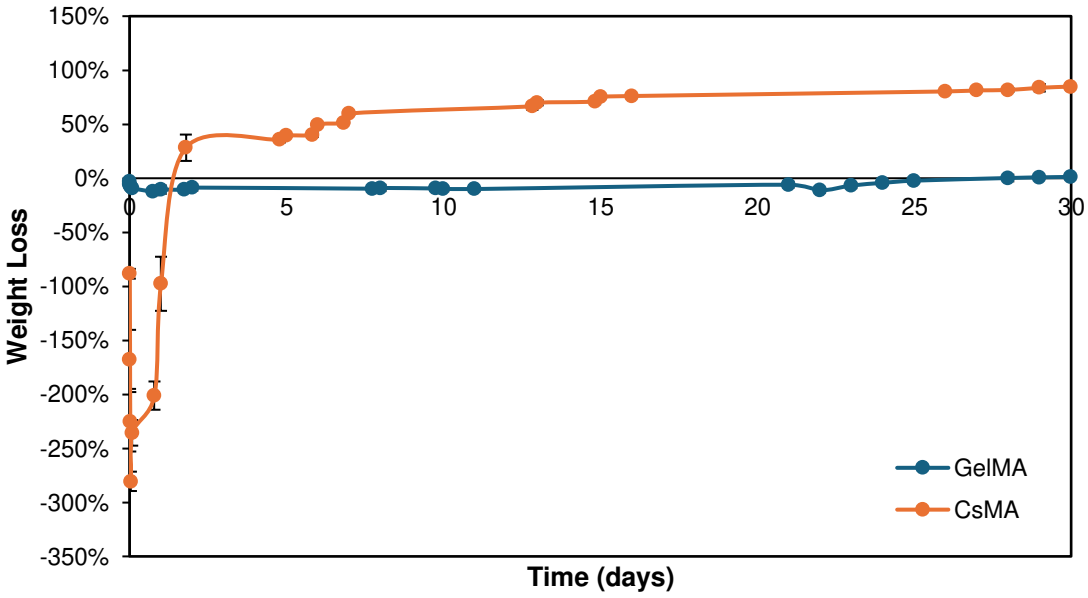

Figure 28 - Weight loss percentage within 30 days of incubation in PBS at 37 ºC of hydrogels of GelMA and CsMA.

The stability test was conducted on two distinct hydrogel formulations: GelMA and CsMA, over a period of 30 days at 37°C, as depicted in Figure 28. The GelMA sample exhibited excellent stability, consistently maintaining its weight loss at approximately 0% from the start of the test. Conversely, the CsMA sample displayed poor stability. Its weight surged dramatically within the first hour, reaching nearly 300% weight gain, then fell below 0% by the second day. Following this, the weight decreased gradually, eventually reaching 85% weight loss by the end of the test.

Due to the statistically significant low stability of CsMA when compared with GelMA (p<0.05), the work was refocused on GelMA. Even the 1:1 GelMA-CsMA mixture did not produce satisfactory results, leading to the decision to continue the investigation exclusively with GelMA. Therefore, the stability of GelMA alone and its respective blends — GelMA4%_Pectin1%, GelMA4%_PEGDA0.5%, and GelMA4%_PEGDA1% — was evaluated.

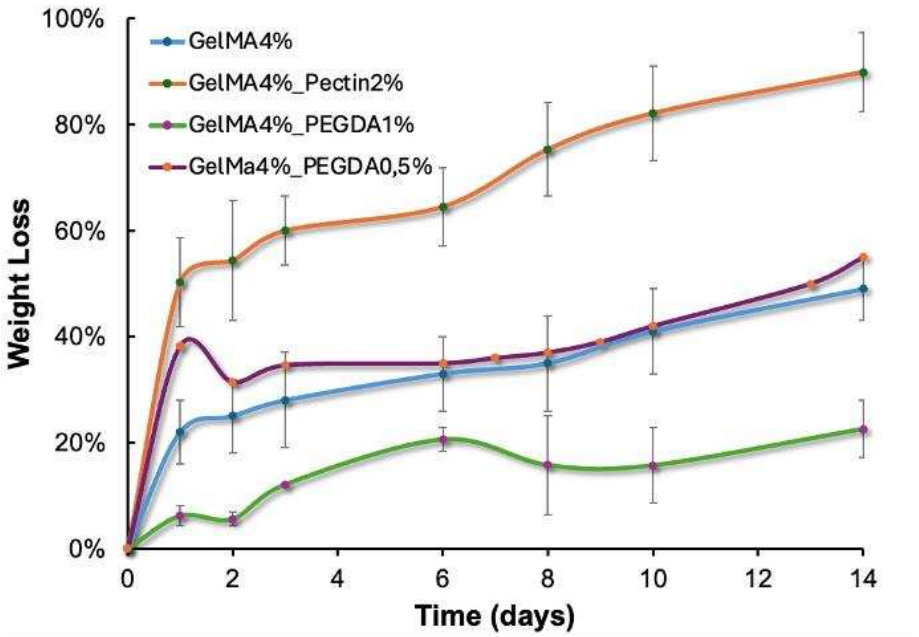

Figure 29 – Weight loss percentage within 14 days of incubation in PBS at 37 ºC of cryogels of GelMA, GelMA_Pectin2% GelMA _PEGDA0.5% and GelMA_PEGDA1%.

The stability test was conducted on cryogels synthesized with GelMA to evaluate the impact of adding 2% Pectin, 0.5% and 1% PEGDA over a 14-days incubation at 37°C, as displayed in Figure 29. The pectin-containing formulation showed almost complete degradation, with nearly 100% weight loss by day 14. The cryogel composed of only GelMA exhibited a moderate weight loss of 40% by the end of the incubation period, as well as the one cointaining 0.5% PEGDA. In contrast, the 1% PEGDA formulation demonstrated the highest stability, with only around 20% weight loss. There were statistically significant differences between the GelMA_Pectin2% formulation and all the other three formulations, and between the GelMA_PEGDA0.5% and the GelMA_PEGDA1% formulations (p<0.05).

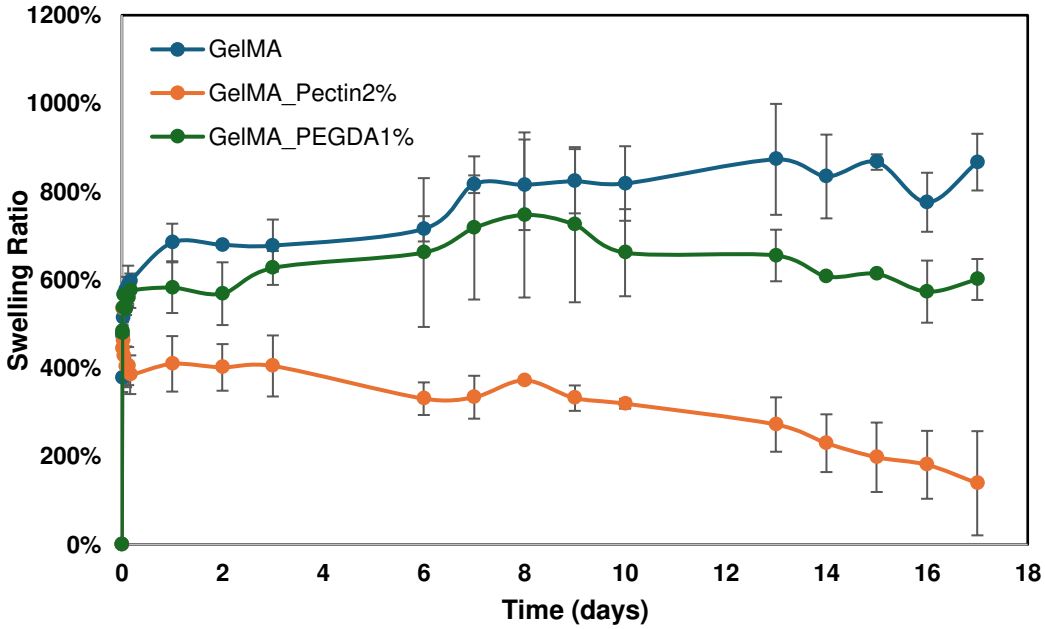

Figure 30 - Swelling ratio percentage within 17 days of incubation in PBS at 37 ºC of cryogels of GelMA, GelMA_Pectin2% and GelMA_PEGDA1%.

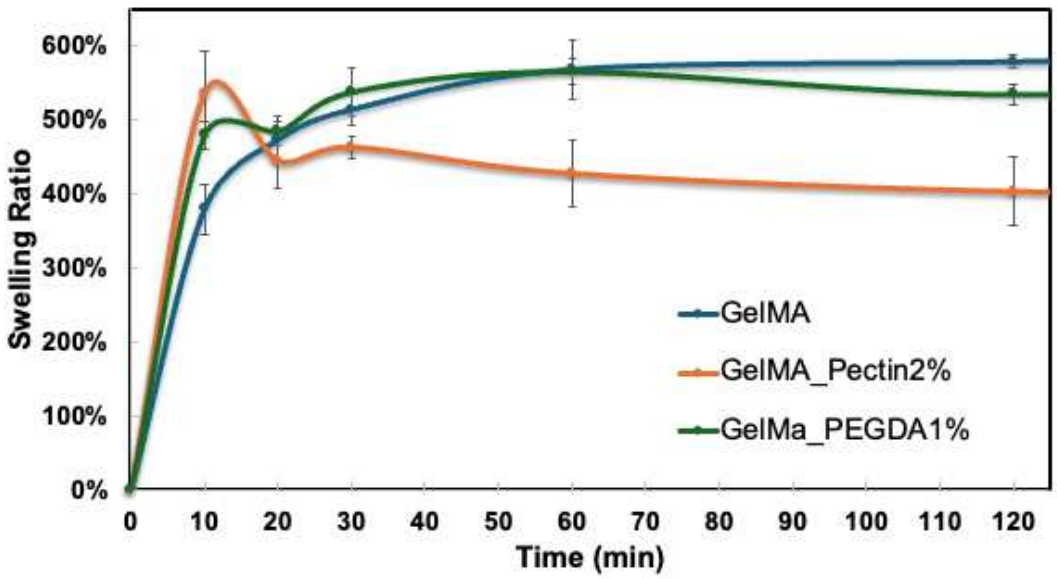

Figure 31 - Swelling ratio percentage in the first 2 hours of incubation in PBS at 37 ºC of cryogels of GelMA, GelMA_Pectin2% and GelMA_PEGDA1%.

The swelling test was carried out on the cryogels synthesized using GelMA, examining the effects of the presence of Pectin (2%) and PEGDA (1%), up to 17 days of incubation at 37˚C (Fig. 30). The formulation with only GelMA showed the highest swelling ratio, with over 800%, followed by the GelMA_PEGDA1% formulation, with roughly 600%. The GelMA_Pectin2% formulation, on the other hand, showed the lowest capacity to hold water, while also having a decreasing trend, unlike the other samples, finishing at about 150%. Overall,

all samples retained a significant amount of water, reaching equilibrium within the first 2 hours of incubation and remaining relatively stable for up to three weeks. The exception was the GelMA_Pectin2% formulation, which began to degrade by day eight. There were statistically significant differences between all three of the formulations (p<0.05), with the GelMA_Pectin2% one being the most different.

3.3. Morphological Characterization

SEM analysis of the transversal sections was used to investigate the microstructure of the GelMA, GelMA_Pectin2%, GelMA_PEGDA1%, and GelMA_PEGDA0.5% cryogel formulations after freeze drying. The SEM images (Fig. 32) show a high porosity for all formulations. In the GelMA formulation (Fig. 32a), fewer pores are observed, but they are larger, exceeding 200 µm in size. In the GelMA_Pectin2% formulation (Fig. 32b), the addition of another polymer, pectin, results in smaller pores, around 120 µm, homogeneously distributed. The addition of PEGDA, both at 1% (Fig. 32c) and 0.5% (Fig. 32d), leads to pores approximately 200 µm in size, also distributed homogeneously.

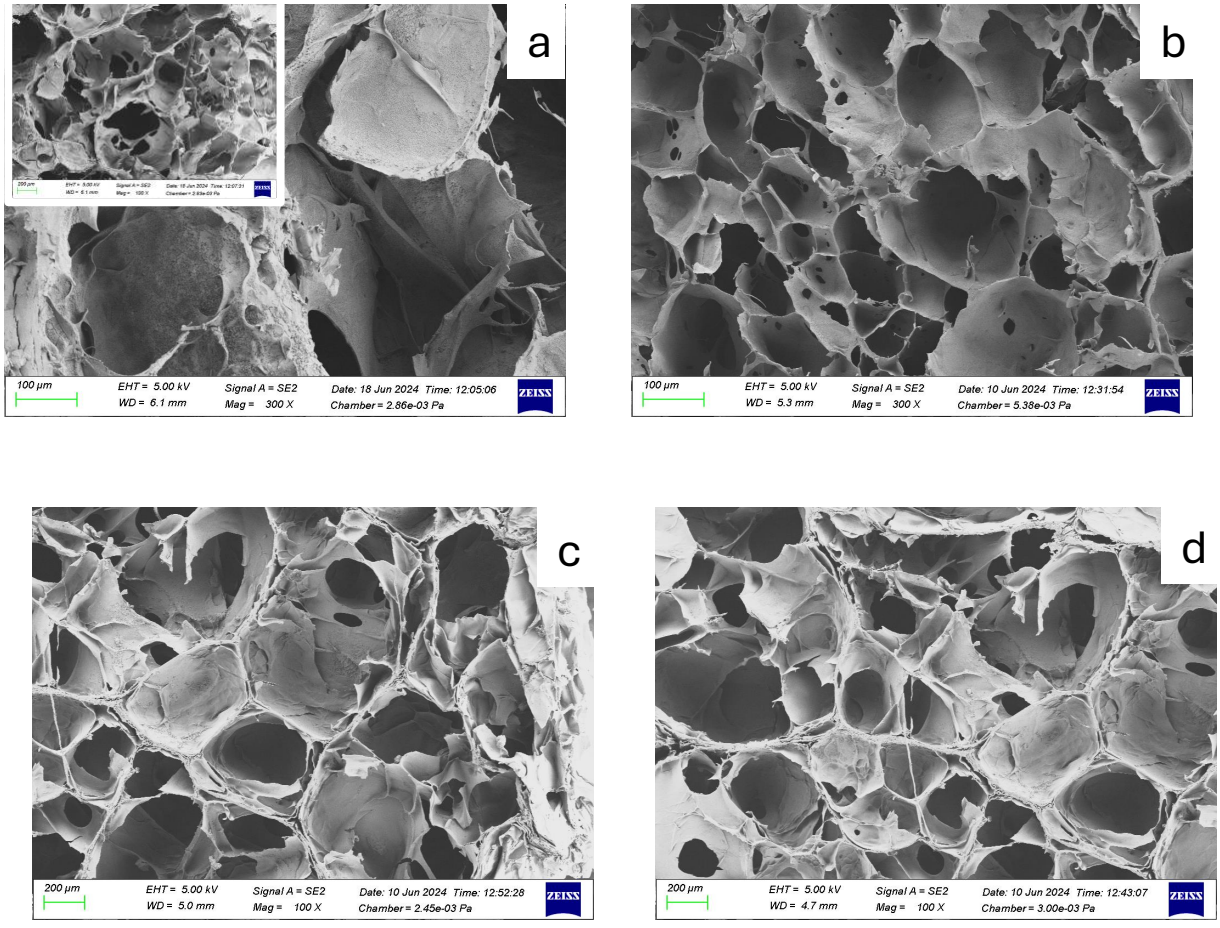

Figure 32 - SEM images of transversal sections of the four cryogel formulations: b) GelMA4%_Pectin2%, c) GelMA4&_PEGDA1%, d) GelMA4%_PEGDA0.5%. All images are at 300x magnification. In image a), a detailed view is shown at 100x magnification.

3.4. Mechanical Behaviour

3.4.1. Rheological Characterization

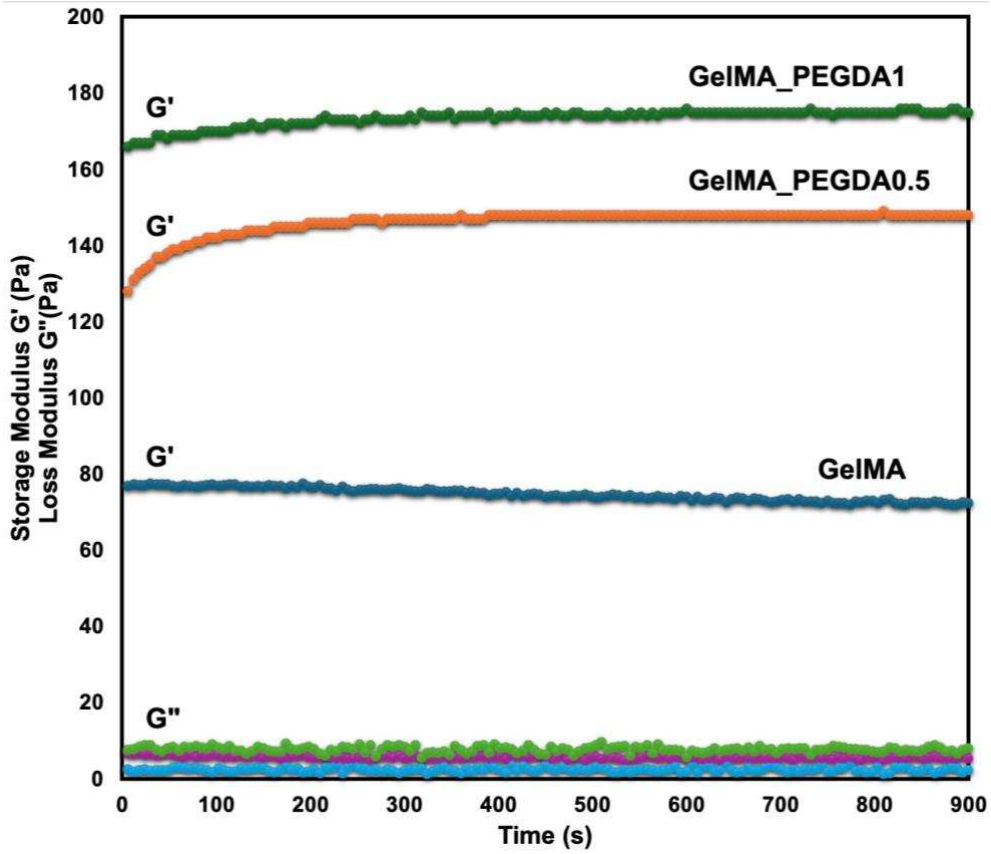

Figure 33 - G' and G" of GelMA, GelMA_PEGDA0.5% and GelMA_PEGDA 1% cryogels over time.

The mechanical properties of cryogels with varying PEGDA concentrations were examined using rheology. The storage and the loss modulus were recorded for 15 min and were found to be almost constant, with an increase only in G'.

As depicted in Figure 33, the G' of GelMA increased with higher PEGDA concentrations. This indicates that incorporating PEGDA enhances the storage modulus of the cryogel, independent of the type of cross-linking (physical interactions) involved. The presence of additional macromolecules in PEGDA appears to strengthen the overall viscoelastic properties of the polymer network. Similar effects have been observed with rheological additives made from polysaccharides or proteins in hydrogels, as well as with the addition of whey protein to gelatin gels [61].

3.4.2. Compression Test

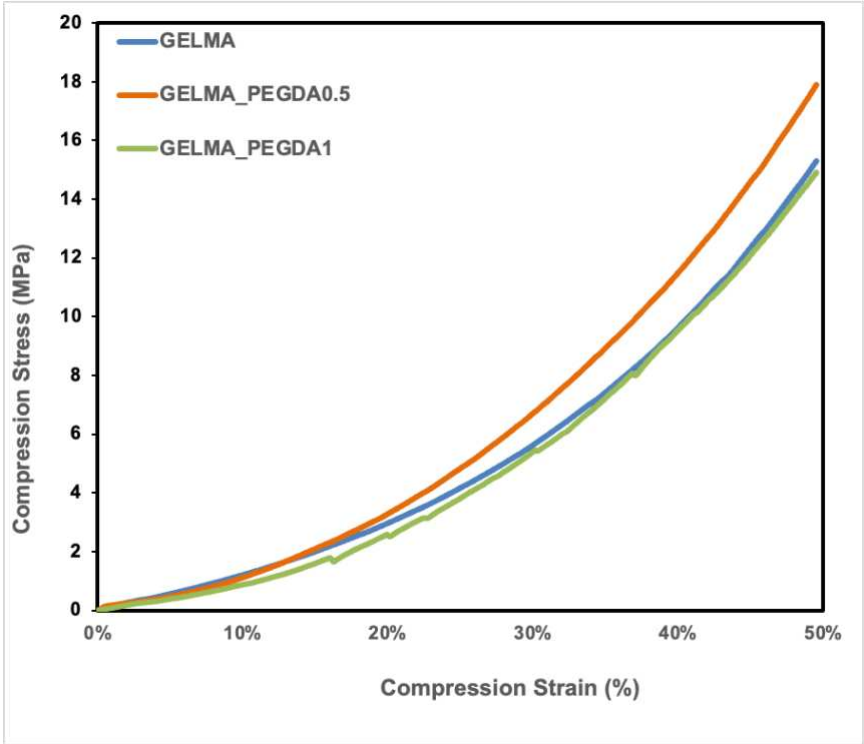

Figure 34 - Compression Stress vs Compression Strain curves for GelMA, GelMA_PEGDA0.5% and GelMA_PEGDA1% cryogels.

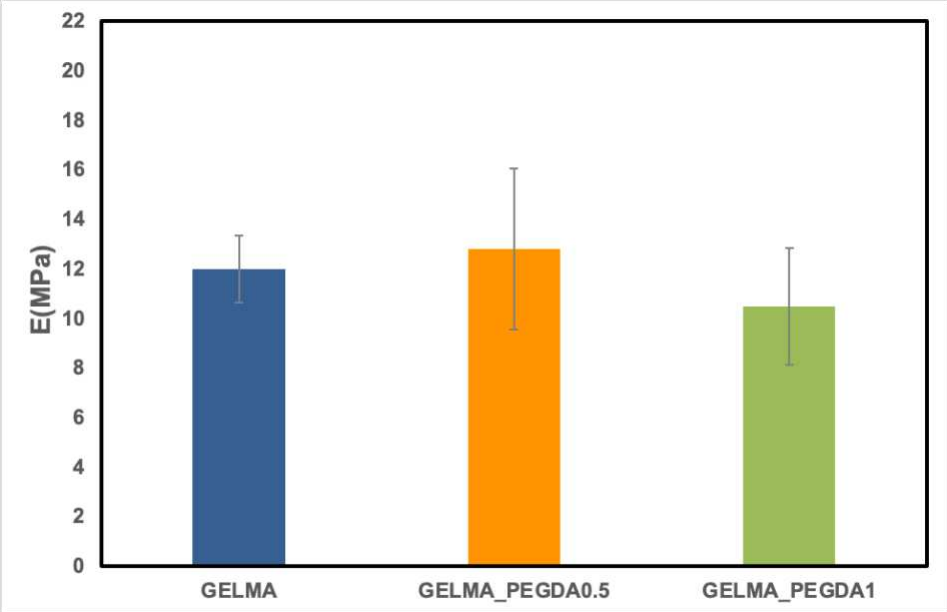

Figure 35 - Young's Moduli (E) for GelMA, GelMA_PEGDA0.5% and GelMA_PEGDA1% cryogels.

Figure 34 shows a typical stress versus strain curve for the GelMA-based scaffolds in their wet state, which suggests that adding PEGDA at 0.5% concentration makes the material stiffer and more resistant to compression. Figure 35 demonstrates that the compressive Young's modulus (E) was similar across all samples (12.0±1.4 MPa for GelMA, 12.8±3.3 MPa for

GelMA_PEGDA0.5% and 10.5±2.4 MPa for GelMA_PEGDA1%). No statistically significant differences were found neither between GelMA and GelMA_PEGDA0.5%, nor between GelMA and GelMA_PEGDA1%, nor between GelMA_PEGDA0.5% and GelMA_PEGDA1% (p>0.05).

One major limitation of using hydrogels for *in vitro* tissue engineering is their generally poor mechanical properties [62]. However, the cryogels developed in this work exhibit compressive Young's moduli up to four orders of magnitude higher than those reported in the literature [63]. When compared to other hydrogels produced via UV crosslinking and with higher GelMA concentrations, the values reported above are superior, indicating that the GelMA cryogels in this work offer enhanced mechanical performance.

3.4.3. Biocompatibility Test

The first experiment was conducted using cryogels that were washed only with PBS. As shown in Figures 36A, 36B, and 36C, which correspond to GelMA, GelMA_PEGDA0.5%, and GelMA_PEGDA1%, a live/dead assay performed on Day 1 revealed predominantly negative results. Most cells were dead, apart from the cryogels containing 1% PEGDA, which exhibited minimal cell viability (Fig. 36A-B-C). Moreover, the culture medium turned yellow shortly after cell seeding, indicating insufficient washing.

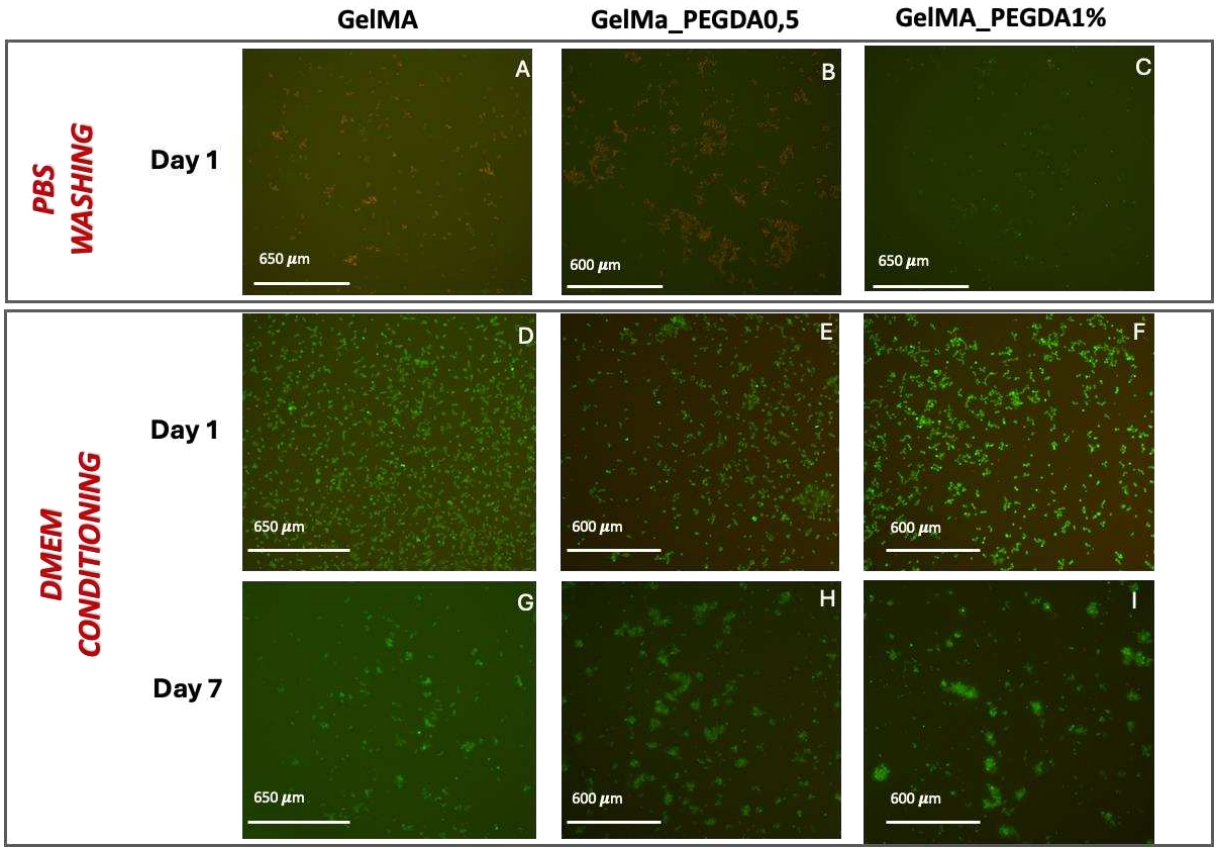

Figure 36 - Biocompatibility tests on GelMA-based cryogels. The first column displays the GelMA cryogels, the second column shows GelMA_PEGDA0.5%, and the third column presents GelMA_PEGDA1%. The images in A, B, and C depict the live/dead assay results for cryogels washed with PBS prior to cell seeding. D, E, F show the results for the same cryogels after a 72-hour preconditioning in DMEM, while G, H, and I illustrate the live/dead assay results after 7 days post-seeding.

Therefore, a second experiment was conducted by adding a preconditioning phase in DMEM for 72 hours before cell seeding. After pre-conditioning the samples in complete DMEM, all cells were alive across all three conditions on day 1 (Fig. 36D-E-F). Greater viability was observed in the GelMA_PEGDA samples, with these results corroborated by images taken on day 7 (Fig. 35H-I).

These findings indicate that the samples require pre-conditioning with culture medium. Cell viability tests are currently underway using the protocol developed here with keratinocyte cells.

4. Discussion

This thesis successfully developed and characterized cryogels based on GelMA, with a focus on evaluating their chemical, physical, morphological, mechanical and biocompatibility properties.

In the initial phase, methacrylated derivatives of gelatin and chitosan were synthesized through methacrylation reactions, with degrees of methacrylation of 55% for GelMA and 16% for CsMA, confirmed using FTIR analysis and a ninhydrin assay. The degree of methacrylation was crucial for crosslinking efficiency: higher methacrylation in GelMA resulted in a denser, more stable cryogel network, whereas the lower degree in CsMA limited its crosslinking and stability, leading to poorer performance in subsequent testing.

Various formulations of GelMA-based cryogels were developed, including the addition of a branched polymer, PEGDA, and a blend with pectin, which could synergistically interact with GelMA. Stability tests showed some differences among the formulations. However, with approximately 40% weight loss after 14 days for both GelMA and GelMA_PEGDA0.5%, the results suggest that the addition of 0.5% PEGDA has a negligible impact on stability. Although no statistically significant differences were observed between GelMA and GelMA_PEGDA1% at a significance level of 0.05, the results approached significance. The GelMA_PEGDA1% formulation demonstrated improved stability, with only 20% weight loss after 14 days. In contrast, GelMA_Pectin2% degraded rapidly, highlighting pectin's unsuitability for applications requiring long-term stability. These findings suggest that PEGDA is more effective than pectin in enhancing cryogel stability.

Swelling tests provided insights into the water absorption and retention abilities of the different formulations, showing statistically significant differences between all the formulations (GelMA, GelMA_Pectin2%, GelMA_PEGDA1%). Adding PEGDA reduced swelling capacity, indicating that increased crosslinking density limits water uptake. This controlled swelling behavior, combined with enhanced stability, positions GelMA_PEGDA cryogels as adaptable materials for applications that require both water retention and mechanical resilience, such as tissue scaffolds where moisture retention is vital for cell survival and proliferation.

SEM imaging provided valuable information on the internal architecture of the cryogels. All formulations exhibited a porous structure, which is essential for cell infiltration, nutrient transport, and waste removal, making it a critical feature for tissue engineering. GelMA cryogels showed larger, interconnected pores, indicating an open network structure that can support greater water retention and cellular growth. The inclusion of PEGDA and pectin formed

smaller, more uniformly distributed pores, with PEGDA resulting in a more controlled and stable porous structure. This architecture is significant for tissue engineering applications, as the scaffold's mechanical properties and biological functionality are influenced by its internal structure.

Mechanical testing revealed insights into the structural integrity of the cryogels and their ability to withstand stress. PEGDA enhanced the viscoelastic properties, evidenced by increased storage modulus, though its effect on compressive stiffness was less pronounced. Both GelMA and GelMA_PEGDA formulations exhibited high compressive strength, with no statistically significant differences between them, suggesting that GelMA cryogels already possess adequate mechanical strength for many applications. PEGDA's primary role may lie in adjusting other cryogel characteristics, such as stability and rheological behaviour. The mechanical robustness of GelMA cryogels positions them as suitable candidates for load-bearing applications like cartilage or bone tissue engineering, where mechanical integrity is essential.

Biocompatibility tests initially faced challenges due to residual cytotoxicity from inadequate washing protocols, which impacted cell viability. However, optimization of the preparation process - including thorough washing, UV sterilization, and cryogel preconditioning in complete DMEM - resulted in excellent cell viability in the final tests, particularly for GelMA_PEGDA samples. Pre-incubation proved crucial for neutralizing residual toxic components, ensuring that the cryogels were biocompatible and conducive to cell adhesion and proliferation. These results highlight the importance of refining preparation and conditioning processes to achieve reliable biocompatibility, a key factor for the successful application of these cryogels in tissue engineering and other biomedical fields.

5. Conclusions

This thesis successfully developed and characterized GelMA-based cryogels, presenting promising advances in cryogel formulations for tissue engineering and osseointegration applications. Through a systematic evaluation of chemical, physical, morphological, mechanical and biocompatibility properties, it was demonstrated that GelMA-based cryogels, especially those modified with PEGDA, exhibit superior stability, controlled swelling, and biocompatibility. These attributes are essential for scaffolding materials aimed at supporting soft tissue integration with osseointegrated lower limb prostheses.

The degree of methacrylation emerged as a pivotal factor for the crosslinking efficiency of both GelMA and CsMA. The relatively high degree of methacrylation in GelMA (55%) facilitated a dense and stable cryogel matrix, whereas the lower methacrylation in CsMA (16%) limited its structural integrity and crosslinking potential, impacting its suitability for load-bearing applications.

In stability tests, the GelMA_PEGDA1% formulation demonstrated lower weight loss over 14 days compared to GelMA alone. Conversely, pectin was found to accelerate degradation rates, indicating its unsuitability for applications requiring prolonged material stability. These findings underscore the role of PEGDA as an effective additive for improving stability, where controlled degradation and reliable mechanical support are critical.

Swelling tests revealed that PEGDA effectively moderates the swelling capacity of GelMA cryogels, creating a balance between crosslinking density and water retention. This tailored swelling behaviour, combined with improved stability, positions GelMA_PEGDA cryogels as versatile materials for applications that demand both water retention and mechanical resilience.

The porous structure observed in SEM imaging further supports this, as it offers a conducive environment for cell infiltration, nutrient transport, and waste removal – all crucial for tissue engineering applications. PEGDA's addition, by creating a uniform and controlled porous network, enhances the scaffold's potential to support cell growth and function within the host tissue.

Mechanical testing indicated that while GelMA cryogels already possess substantial compressive strength, PEGDA enhances their viscoelastic properties without compromising mechanical integrity, suggesting suitability for load-bearing applications. This finding is particularly relevant for the development of cryogels in cartilage and bone tissue engineering, where both resilience to compressive forces and structural stability are vital.

The optimization of preparation and conditioning protocols in biocompatibility testing was instrumental in achieving high cell viability and ensuring compatibility, especially of GelMA_PEGDA cryogels. By refining washing, UV sterilization, and preconditioning processes, residual cytotoxicity was minimized, supporting cellular adhesion and proliferation. This is a crucial step for the practical application of these cryogels in biomedical fields, where reliable biocompatibility is essential for successful integration with host tissue.

Overall, the outcomes of this work highlight GelMA_PEGDA cryogels as adaptable, biocompatible, and mechanically robust scaffolds suitable for various tissue engineering applications. The successful synthesis and optimization of these cryogel formulations contribute valuable insights into the design of biomaterials that enhance soft tissue integration with osseointegrated lower limb prostheses, ultimately advancing prosthetic development and improving the quality of life for individuals with lower limb amputations.

6. Future Work

Moving forward, several key areas warrant further investigation to fully realize the potential of these materials in biomedical applications.

First, a more comprehensive mechanical characterization is needed. Apart from the rheological and compressive tests carried out in the present work, it is also recommended that tensile tests be done in order to determine elasticity and tensile strength of the cryogels. These properties are important in the consideration of how such materials would withstand the mechanical strains of soft tissue attachment to osseointegrated limb prostheses which require a considerable degree of flexibility and durability.

Second, biocompatibility tests should be expanded. While this work demonstrated good initial cell viability after optimizing the pre-conditioning protocol, future tests should focus on long-term cell proliferation and the morphology of specific cell types, such as fibroblasts or keratinocytes. These cells are key to the successful integration of the cryogels with skin and connective tissues, and their behavior on the cryogel surface will provide insights into the material's suitability for clinical applications. Furthermore, incorporating live/dead assays with proliferation markers and immunostaining for cytoskeletal and adhesion proteins could provide a more detailed understanding of cell-material interactions.

Additionally, exploring bioactive enhancements to the GelMA_PEGDA cryogels may further improve their performance. For instance, incorporating growth factors, peptides, or extracellular matrix components could enhance cell adhesion, proliferation, and tissue regeneration. These modifications could make the material even more suitable for the interface for soft tissue with prosthetic devices.

Finally, *in vivo* studies will be crucial for translating these materials from the lab to clinical applications. Animal models could be used to evaluate the biocompatibility, integration, and mechanical performance of the cryogels in a living system, providing a clearer picture of their potential for human use.

By expanding mechanical and biocompatibility testing, incorporating bioactive enhancements, and moving towards *in vivo* validation, these GelMA-based cryogels hold significant promise for advancing tissue engineering and prosthetic integration technologies.

7. References

[1] Fishman, S. (1977). Education in prosthetics and orthotics. *Prosthetics and Orthotics International*, *1*(1), 52-55.

[2] Webster, J. B., Bachus, K. N., Beck, J. P., Jeyapalina, S., Drew, A. J., & Bloebaum, R. D. (2017). Osseointegration research. *Full Stride: Advancing the State of the Art in Lower Extremity Gait Systems*, 167-193.

[3] Maryniak, A., Laschowski, B., & Andrysek, J. (2018). Technical overview of osseointegrated transfemoral prostheses: Orthopedic surgery and implant design centered. *Journal of Engineering and Science in Medical Diagnostics and Therapy*, *1*(2), 020801.

[4] Overmann, A. L., & Forsberg, J. A. (2020). The state of the art of osseointegration for limb prosthesis. *Biomedical engineering letters*, *10*(1), 5-16.

[5] Hagberg, K., Brånemark, R., Gunterberg, B., & Rydevik, B. (2008). Osseointegrated trans-femoral amputation prostheses: prospective results of general and condition-specific quality of life in 18 patients at 2-year follow-up. *Prosthetics and orthotics international*, *32*(1), 29-41.

[6] Brånemark, R., Berlin, Ö., Hagberg, K., Bergh, P., Gunterberg, B., & Rydevik, B. (2014). A novel osseointegrated percutaneous prosthetic system for the treatment of patients with transfemoral amputation: A prospective study of 51 patients. *The bone & joint journal*, *96*(1), 106-113.

[7] Hagberg, K., & Brånemark, R. (2009). One hundred patients treated with osseointegrated transfemoral amputation prostheses--rehabilitation perspective. *Journal of Rehabilitation Research & Development*, *46*(3).

[8] Thesleff, A., Brånemark, R., Håkansson, B., & Ortiz-Catalan, M. (2018). Biomechanical characterisation of bone-anchored implant systems for amputation limb prostheses: a systematic review. *Annals of biomedical engineering*, *46*, 377-391.

[9] McGough, R. L., Goodman, M. A., Randall, R. L., Forsberg, J. A., Potter, B. K., & Lindsey, B. (2017). The Compress® transcutaneous implant for rehabilitation following limb amputation. *Der Unfallchirurg*, *120*(4), 300-305.

[10] Pedtke, A. C., Wustrack, R. L., Fang, A. S., Grimer, R. J., & O'Donnell, R. J. (2012). Aseptic failure: how does the Compress® implant compare to cemented stems?. *Clinical Orthopaedics and Related Research®*, *470*(3), 735-742.

[11] Zimel, M. N., Farfalli, G. L., Zindman, A. M., Riedel, E. R., Morris, C. D., Boland, P. J., & Healey, J. H. (2016). Revision distal femoral arthroplasty with the Compress® prosthesis has a low rate of mechanical failure at 10 years. *Clinical Orthopaedics and Related Research®*, *474*(2), 528-536.

[12] Korabi, R., Shemtov-Yona, K., & Rittel, D. (2017). On stress/strain shielding and the material stiffness paradigm for dental implants. *Clinical implant dentistry and related research*, *19*(5), 935-943.

[13] Denard, P. J., Raiss, P., Gobezie, R., Edwards, T. B., & Lederman, E. (2018). Stress shielding of the humerus in press-fit anatomic shoulder arthroplasty: review and recommendations for evaluation. *Journal of shoulder and elbow surgery*, *27*(6), 1139-1147.

[14] McGough, R. L., Goodman, M. A., Randall, R. L., Forsberg, J. A., Potter, B. K., & Lindsey, B. (2017). The Compress® transcutaneous implant for rehabilitation following limb amputation. *Der Unfallchirurg*, *120*(4), 300-305.

[15] Huiskes, R. I. K., Weinans, H., & Van Rietbergen, B. (1992). The relationship between stress shielding and bone resorption around total hip stems and the effects of flexible materials. *Clinical Orthopaedics and Related Research®*, *274*, 124-134.

[16] Kagan, R., Adams, J., Schulman, C., Laursen, R., Espana, K., Yoo, J., ... & Hayden, J. (2017). What factors are associated with failure of compressive osseointegration fixation?. *Clinical Orthopaedics and Related Research®*, *475*(3), 698-704.

[17] Tyler, W. K., Healey, J. H., Morris, C. D., Boland, P. J., & O'Donnell, R. J. (2009). Compress® periprosthetic fractures: interface stability and ease of revision. *Clinical Orthopaedics and Related Research®*, *467*, 2800-2806.

[18] Kancherla, V. K., Del Gaizo, D. J., Paprosky, W. G., & Sporer, S. M. (2014). Utility of trephine reamers in revision hip arthroplasty. *The Journal of Arthroplasty*, *29*(1), 210-213.

[19] Juhnke, D. L., Beck, J. P., & Aschoff, H. H. (2015). Fifteen years of experience with Integral-Leg-Prosthesis: Cohort study of artificial limb attachment system. *Journal of Rehabilitation Research and Development*, *52*(4), 407.

[20] Frölke, J. P. M., Leijendekkers, R. A., & Van de Meent, H. (2017). Osseointegrated prosthesis for patients with an amputation: Multidisciplinary team approach in the Netherlands. *Der Unfallchirurg*, *120*(4), 293.

[21] Al Muderis, M., Lu, W., & Li, J. J. (2017). Osseointegrated Prosthetic Limb for the treatment of lower limb amputations: Experience and outcomes. *Der Unfallchirurg*, *120*(4), 306-311.

[22] Al Muderis, M., Khemka, A., Lord, S. J., Van de Meent, H., & Frölke, J. P. M. (2016). Safety of osseointegrated implants for transfemoral amputees: a two-center prospective cohort study. *JBJS*, *98*(11), 900-909.

[23] Al Muderis, M., Tetsworth, K., Khemka, A., Wilmot, S., Bosley, B., Lord, S. J., & Glatt, V. (2016). The Osseointegration Group of Australia Accelerated Protocol (OGAAP-1) for two-stage osseointegrated reconstruction of amputated limbs. *The bone & joint journal*, *98*(7), 952-960.

[24] Pendegrass, C. J., Tucker, B., Patel, S., Dowling, R., & Blunn, G. W. (2012). The effect of adherens junction components on keratinocyte adhesion in vitro: Potential implications for sealing the skin-implant interface of intraosseous transcutaneous amputation prostheses. *Journal of Biomedical Materials Research Part A*, *100*(12), 3463-3471.

[25] Roffman, C. E., Buchanan, J., & Allison, G. T. (2014). Predictors of non-use of prostheses by people with lower limb amputation after discharge from rehabilitation: development and validation of clinical prediction rules. *Journal of physiotherapy*, *60*(4), 224-231.

[26] Durmus, D., Safaz, I., Adıgüzel, E., Uran, A., Sarısoy, G., Goktepe, A. S., & Tan, A. K. (2015). The relationship between prosthesis use, phantom pain and psychiatric symptoms in male traumatic limb amputees. *Comprehensive Psychiatry*, *59*, 45-53.

[27] Meulenbelt, H. E., Geertzen, J. H., Jonkman, M. F., & Dijkstra, P. U. (2009). Determinants of skin problems of the stump in lower-limb amputees. *Archives of physical medicine and rehabilitation*, *90*(1), 74-81.

[28] Sanders, J. E., & Fatone, S. (2011). Residual limb volume change: systematic review of measurement and management. *Journal of rehabilitation research and development*, *48*(8), 949.

[29] Ghoseiri, K., & Safari, R. (2014). Prevalence of heat and perspiration discomfort inside prostheses: literature review. *Journal of rehabilitation research and development*.

[30] Kunutsor, S. K., Gillatt, D., & Blom, A. W. (2018). Systematic review of the safety and efficacy of osseointegration prosthesis after limb amputation. *Journal of British Surgery*, *105*(13), 1731-1741.

[31] Pi, B. (1977). Osseointegrated implants in the treatment of the edentulous jaw. Experience from a 10 year period. *Scand J Plast Reconstr Surg Suppl*, *16*, 1-132.

[32] Worthington, P. (1997). History, development, and current status of osseointegration as revealed by experience in craniomaxillofacial surgery. *Osseointegration in skeletal reconstruction and joint replacement. Carol Stream, IL: Quintessence Publishing Co*, 25-44.

[33] Brånemark, P. I. (1959). Vital microscopy of bone marrow in rabbit. *Scand J Clin Lab Invest*, *38*(11), 1.

[34] Hebert, J. S., Rehani, M., & Stiegelmar, R. (2017). Osseointegration for lower-limb amputation: a systematic review of clinical outcomes. *JBJS reviews*, *5*(10), e10.

[35] Chimutengwende-Gordon, M., Dowling, R., Pendegrass, C., & Blunn, G. (2018). Determining the porous structure for optimal soft-tissue ingrowth: an in vivo histological study. *PLoS One*, *13*(10), e0206228.

[36] Chimutengwende-Gordon, M., Pendegrass, C., & Blunn, G. (2011). Enhancing the soft tissue seal around intraosseous transcutaneous amputation prostheses using silanized fibronectin titanium alloy. *Biomedical Materials*, *6*(2), 025008.

[37] Chimutengwende-Gordon, M., Pendegrass, C., & Blunn, G. (2017). The in vivo effect of a porous titanium alloy flange with hydroxyapatite, silver and fibronectin coatings on soft-tissue integration of intraosseous transcutaneous amputation prostheses. *The bone & joint journal*, *99*(3), 393-400.

[38] Wang, X., Lei, X., Yu, Y., Miao, S., Tang, J., Fu, Y., ... & Ding, J. (2021). Biological sealing and integration of a fibrinogen-modified titanium alloy with soft and hard tissues in a rat model. *Biomaterials Science*, *9*(15), 5192-5208.

[39] Pendegrass, C. J., Gordon, D., Middleton, C. A., Sun, S. N. M., & Blunn, G. W. (2008). Sealing the skin barrier around transcutaneous implants: in vitro study of keratinocyte proliferation and adhesion in response to surface modifications of titanium alloy. *The Journal of Bone & Joint Surgery British Volume*, *90*(1), 114-121.

[40] Pitkin, M., Raykhtsaum, G., Galibin, O. V., Protasov, M. V., Chihovskaya, J. V., & Belyaeva, I. G. (2006). Skin and bone integrated prosthetic pylon: A pilot animal study. *Journal of rehabilitation research and development*, *43*(4), 573.

[41] Holt, B. M., Bachus, K. N., Beck, J. P., Bloebaum, R. D., & Jeyapalina, S. (2013). Immediate post-implantation skin immobilization decreases skin regression around percutaneous osseointegrated prosthetic implant systems. *Journal of biomedical materials research Part A*, *101*(7), 2075-2082.

[42] Kou, S. G., Peters, L. M., & Mucalo, M. R. (2021). Chitosan: A review of sources and preparation methods. *International Journal of Biological Macromolecules*, *169*, 85-94.

[43] Thakur, V. K., & Thakur, M. K. (2014). Recent advances in graft copolymerization and applications of chitosan: a review. *ACS Sustainable Chemistry & Engineering*, *2*(12), 2637-2652.

[44] Ropartz, D., & Ralet, M. C. (2020). Pectin structure. *Pectin: Technological and physiological properties*, 17-36.

[45] Neumann, N., Thinius, S., Abels, G., Hartwig, A., Koschek, K., & Boskamp, L. (2023). Multifunctional hyperbranched prepolymers with tailored degree of methylation and methacrylation. *Polymer*, *276*, 125886.

[46] Cebe, T., Ahuja, N., Monte, F., Awad, K., Vyavhare, K., Aswath, P., ... & Varanasi, V. (2020). Novel 3D-printed methacrylated chitosan-laponite nanosilicate composite scaffolds enhance cell growth and biomineral formation in MC3T3 pre-osteoblasts. *Journal of materials research*, *35*(1), 58-75.

[47] Wong, T. W., Wu, J., Yang, M., Kadir, M. R. A., Wahit, M. U., & Zhao, Q. (2017). Multifunctional shape-memory foams with highly tunable properties via organo-phase cryo-polymerization. *Journal of Materials Chemistry A*, *5*(20), 9793-9800.

[48] Park, J., Kwon, S., Hwang, N. S., & Kang, B. J. (2018). Clinical application of bone morphogenetic protein-2 microcarriers fabricated by the cryopolymerization of gelatin methacrylate for the treatment of radial fracture in two dogs. *in vivo*, *32*(3), 575-581.

[49] Park, J., Kwon, S., Hwang, N. S., & Kang, B. J. (2018). Clinical application of bone morphogenetic protein-2 microcarriers fabricated by the cryopolymerization of gelatin methacrylate for the treatment of radial fracture in two dogs. *in vivo*, *32*(3), 575-581.

[50] Ribas-Massonis, A., Cicujano, M., Duran, J., Besalú, E., & Poater, A. (2022). Free-radical photopolymerization for curing products for refinish coatings market. *Polymers*, *14*(14), 2856.

[51] Tajau, R., Ibrahim, M. I., Yunus, N. M., Mahmood, M. H., Salleh, M. Z., & Salleh, N. G. N. (2014, February). Development of palm oil-based UV-curable epoxy acrylate and urethane acrylate resins for wood coating application. In *AIP Conference Proceedings* (Vol. 1584, No. 1, pp. 164-169). American Institute of Physics.

[52] Kolawole, O. M., Lau, W. M., & Khutoryanskiy, V. V. (2018). Methacrylated chitosan as a polymer with enhanced mucoadhesive properties for transmucosal drug delivery. *International Journal of Pharmaceutics*, *550*(1-2), 123-129.

[53] Dutta, A. (2017). Fourier transform infrared spectroscopy. *Spectroscopic methods for nanomaterials characterization*, 73-93.

[54] Friedman, M. (2004). Applications of the ninhydrin reaction for analysis of amino acids, peptides, and proteins to agricultural and biomedical sciences. *Journal of agricultural and food chemistry*, *52*(3), 385-406.

[55] Zatorski, J. M., Montalbine, A. N., Ortiz-Cárdenas, J. E., & Pompano, R. R. (2020). Quantification of fractional and absolute functionalization of gelatin hydrogels by optimized ninhydrin assay and 1 H NMR. *Analytical and bioanalytical chemistry*, *412*, 6211-6220.

[56] Park, J., Kwon, S., Hwang, N. S., & Kang, B. J. (2018). Clinical application of bone morphogenetic protein-2 microcarriers fabricated by the cryopolymerization of gelatin methacrylate for the treatment of radial fracture in two dogs. *in vivo*, *32*(3), 575-581.

[57] Modaresifar, K., Hadjizadeh, A., & Niknejad, H. (2018). Design and fabrication of GelMA/chitosan nanoparticles composite hydrogel for angiogenic growth factor delivery. *Artificial cells, nanomedicine, and biotechnology*, *46*(8), 1799-1808.

[58] Morello, G., Polini, A., Scalera, F., Rizzo, R., Gigli, G., & Gervaso, F. (2021). Preparation and characterization of salt-mediated injectable thermosensitive chitosan/pectin hydrogels for cell embedding and culturing. *Polymers*, *13*(16), 2674.

[59] Mohammed, A., & Abdullah, A. (2018, November). Scanning electron microscopy (SEM): A review. In *Proceedings of the 2018 International Conference on Hydraulics and Pneumatics—HERVEX, Băile Govora, Romania* (Vol. 2018, pp. 7-9).

[60] de Moura, M. R., Aouada, F. A., & Mattoso, L. H. (2008). Preparation of chitosan nanoparticles using methacrylic acid. *Journal of colloid and interface science*, *321*(2), 477-483.

[61] Kirsch, M., Birnstein, L., Pepelanova, I., Handke, W., Rach, J., Seltsam, A., ... & Lavrentieva, A. (2019). Gelatin-methacryloyl (GelMA) formulated with human platelet lysate supports mesenchymal stem cell proliferation and differentiation and enhances the hydrogel's mechanical properties. *Bioengineering*, *6*(3), 76.

[62] Petrini, P., Fare, S., Piva, A., & Tanzi, M. C. (2003). Design, synthesis and properties of polyurethane hydrogels for tissue engineering. *Journal of materials Science: materials in medicine*, *14*, 683-686.

[63] Wu, Y., Xiang, Y., Fang, J., Li, X., Lin, Z., Dai, G., ... & Zhang, D. (2019). The influence of the stiffness of GelMA substrate on the outgrowth of PC12 cells. *Bioscience reports*, *39*(1), BSR20181748.